






Proliferation of *Chondrodonta* as a proxy of environmental instability at the onset of OAE1a: Insights from shallow-water limestones of the Apulia Carbonate Platform

GABRIELLA DEL VISCIO* , GIANLUCA FRIJIA*, RENATO POSENATO*, PULKIT SINGH†, DANIEL J. LEHRMANN‡ , JONATHAN L. PAYNE†, KHALID AL-RAMADAN§, ULRICH STRUCK¶ , KLAUS P. JOCHUM**  and MICHELE MORSILLI* 

*Dipartimento di Fisica e Scienze della Terra, Università di Ferrara, Ferrara, 44122, Italy (E-mail: mrrh@unife.it)

†Department of Geological Sciences, Stanford University, Stanford, CA, 94305, USA

‡Department of Geosciences, Trinity University, San Antonio, TX, 78212, USA

§College of Petroleum Engineering & Geosciences, King Fahd University of Petroleum & Minerals, Dhahran, 31261, Saudi Arabia

¶Museum für Naturkunde, Leibniz Institute for Evolution and Biodiversity Science, Berlin, 10115, Germany

**Climate Geochemistry Department, Max Planck Institute for Chemistry (Otto-Hahn-Institute), Mainz, 55020, Germany

Associate Editor – Gregor Eberli

ABSTRACT

Chondrodonta is an opportunistic, oyster-like bivalve, common in shallow-water carbonates of the Cretaceous Tethyan Realm. Despite its high abundance and widespread geographic distribution, the precise relationship between the early Aptian proliferation and environmental perturbations resulting from the Oceanic Anoxic Event 1a (OAE1a), has not been investigated. Stratigraphic and geochemical analyses of the lower Aptian *Chondrodonta* bedsets within the inner platform limestones of the Apulia Carbonate Platform (Gargano Promontory, southern Italy) are conducted to assess the environmental controls on the *Chondrodonta* proliferation and its timing and causal relationship to OAE1a. *Chondrodonta* occurs with sparse to common individuals within requieniid rudist floatstone–rudstones, forms monospecific biostromes during the early phase of stressed environmental conditions and then rapidly disappears at the peak of OAE1a. It proliferates in dysoxic seawater with relatively increased trophic sources, which correlate to increasing nutrient levels in the nearby pelagic realm. *Chondrodonta*-rich beds are associated worldwide with the onset of OAE1a and occur in a transitional context between a stable and a strongly stressed environment, where the opportunistic behaviour of *Chondrodonta* is rather efficient. Increasing nutrient load and unstable environmental conditions right below the peak of OAE1a created an environmental ‘window’ favourable for *Chondrodonta* to proliferate, outplaying the less tolerant benthos (for example, rudists). The occurrence, duration and position of the environmental window were controlled by local palaeogeographic and hydrodynamic settings (i.e. low energy, decreased seawater oxygenation and circulation). Further increase in inhospitable conditions, leading to OAE1a, constituted an upper threshold for *Chondrodonta* and allowed mesotrophic taxa like *Bacinella*–*Lithocodium* and orbitolinids to dominate the benthic

communities. The present study suggests that the proliferation of *Chondrodonta* in shallow-water platform carbonates can be used as proxy for the initial phase of ecological stress related to OAE1a.

Keywords Apulia Carbonate Platform, *Chondrodonta*, early Aptian, OAE1a, Tethys.

INTRODUCTION

Chondrodonta Stanton, 1901, is an epifaunal, filter-feeding, oyster-like bivalve, common in shallow-water carbonates of the Cretaceous Tethyan Realm. It has a gregarious and cemented life-habit with a ‘mud-sticker’ strategy of bottom stabilization (Posenato *et al.*, 2020). Its dense aggregates (bivalve bouquets, thickets and carpets) influenced the sedimentation rates and dynamics of carbonate platform systems (Gili *et al.*, 1995; Skelton & Gili, 2012). *Chondrodonta* has a discontinuous distribution spanning from the ?Berriasian (Masse *et al.*, 2015) to the ?Campanian (Freneix & Lefèvre, 1967) and an abundance peak during the Aptian – Cenomanian interval (Posenato *et al.*, 2018, 2020). *Chondrodonta* accumulations occur worldwide (Dhondt & Dieni, 1993) in a set of marine sub-environments including tidal flats, lagoons, back-reefs and platform margins. The bivalve occurs both in monospecific biostromes (Phelps *et al.*, 2014; Posenato *et al.*, 2018) and associated with rudists (Bover-Arnal *et al.*, 2010; Posenato *et al.*, 2020). *Chondrodonta* is considered an r-strategist and its proliferation around the Cretaceous Oceanic Anoxic Events (OAEs) has been interpreted as evidence of population blooms in response to environmental instability (Graziano, 2013; Posenato *et al.*, 2018, 2020; Núñez-Useche *et al.*, 2020).

During the early Aptian, *Chondrodonta* beds are reported in several shallow-water carbonate platforms bordering the Tethys Ocean (e.g. Masse, 1993; Császár *et al.*, 1994; Malchus *et al.*, 1995; Immenhauser *et al.*, 2004; Gili *et al.*, 2016; Graziano & Raspini, 2018; Posenato *et al.*, 2018, among others) and the proto-North Atlantic (e.g. Phelps *et al.*, 2014; Núñez-Useche *et al.*, 2020).

The early Aptian represents a period of considerable climate and environmental change (Föllmi, 2012) primarily linked to the emplacement of the Ontong Java Large Igneous Province (LIP) in the Pacific Ocean (Larson & Erba, 1999; Tejada *et al.*, 2009). The large amount of CO₂ released into the atmosphere and dissolved in seawater mainly by submarine and subaerial volcanic activity

(Föllmi, 2012; Erba *et al.*, 2015) and, secondly, by methane hydrate dissociation (Méhay *et al.*, 2009), triggered a sequence of climate disturbances that caused crises in carbonate production in both the pelagic and neritic domains (e.g. Erba, 1994; Weissert *et al.*, 1998). The resulting early Aptian OAE1a (i.e. Selli Event – Schlanger & Jenkyns, 1976; Jenkyns, 2010) is associated with a negative $\delta^{13}\text{C}$ spike linked to increased volcanism, followed by a positive $\delta^{13}\text{C}$ excursion (Menegatti *et al.*, 1998; Tejada *et al.*, 2009). The onset of the $\delta^{13}\text{C}$ excursion coincides with widespread black shale deposition in basinal settings and with the nannoconid crisis (Erba, 1994; Erba & Tremolada, 2004).

In shallow-water settings, there is global evidence for a profound environmental change before and during the C-cycle perturbation corresponding to OAE1a. Carbonate platforms within and outside the Tethys underwent significant phases of ecological stress, primarily due to enhanced nutrient input, that resulted in biotic turnovers from oligotrophic to mesotrophic and even to eutrophic communities (e.g. Millán *et al.*, 2009; Skelton & Gili, 2012; Stein *et al.*, 2012).

The shallow-marine carbonate platform ecosystems along the Northern Tethyan margin (e.g. Föllmi *et al.*, 2006; Bover-Arnal *et al.*, 2009; Huck *et al.*, 2013) and in the proto-North Atlantic (e.g. Millán *et al.*, 2011; Huck *et al.*, 2014) drowned, resulting in the deposition of condensed sequences and extensive formation of hardgrounds immediately before and during OAE1a (Godet, 2013). Conversely, carbonate platforms of the Central and Southern Tethys (for example, Croatia and Oman) continued to grow under highly stressed conditions, as indicated by episodes of *Bacinnella*–*Lithocodium* and orbitolinid mass occurrences replacing coral–rudist associations (Huck *et al.*, 2010; Rameil *et al.*, 2010; Schröder *et al.*, 2010; Godet *et al.*, 2014; Hueter *et al.*, 2019, 2020).

The proliferation of the opportunistic *Chondrodonta* in the early Aptian has been interpreted as an indication of unstable environmental conditions during OAE1a, with episodic increases in

food sources and ocean temperature coupled with acidification (Graziano, 2013; Posenato *et al.*, 2018). Despite the high abundance and widespread geographic distribution of *Chondrodonta* (Posenato *et al.*, 2018), a clear cause–effect relationship between its flourishing and OAE1a has yet to be established. Further, it is still unclear whether and how the environmental disturbances linked to the mass release of CO₂ may have played a role in its proliferation and dominance over other bivalve groups (for example, rudists).

The lower Aptian *Chondrodonta* beds of the inner platform facies of the Apulia Carbonate Platform (ACP) are here analysed to determine the temporal relationship between their deposition and the onset of OAE1a. Sedimentological, petrographic and biostratigraphic analyses of stratigraphic sections are integrated and coupled with analyses of geochemical environmental proxies. Results are correlated with the major environmental perturbations recorded in the adjacent Adriatic/Ionian Basin. The stratigraphic position of the *Chondrodonta* beds is further compared to other coeval *Chondrodonta* accumulations to highlight the precise stratigraphic position and the ecological significance of *Chondrodonta* accumulations in relation to the biotic turnovers from oligotrophic to mesotrophic associations recorded during OAE1a.

STRATIGRAPHIC SETTINGS

The Gargano Promontory (Fig. 1A) represents the north-eastern margin of the ACP, a major Mesozoic palaeogeographic domain in the central Tethys (Eberli *et al.*, 1993; Bernoulli, 2001). The Promontory was partially involved in the Neogene southern Apennines and Dinaric thrust belts and is currently interpreted as a deformed foreland (Bosellini *et al.*, 1999a; Borgomano, 2000; Morsilli *et al.*, 2017). It is folded in a gentle and broad north-west/south-east anticline and dissected by Miocene – Pliocene reverse and normal faults, and by Pleistocene strike–slip faults (Bertotti *et al.*, 1999; Brankman & Aydin, 2004). The outcropping carbonate succession records a suite of depositional environments from inner platform and peritidal settings to relatively deep-water pelagic environments (Morsilli & Bosellini, 1997; Borgomano, 2000).

The studied succession belongs to the Lower Cretaceous inner platform facies of the San Giovanni Rotondo Limestone (SGRL) (Luperto Sinni & Masse, 1986; Di Palma, 1995; Claps *et al.*,

1996; Graziano *et al.*, 2013). The SGRL crops out in the eastern and south-eastern Gargano Promontory (Fig. 1A) and changes eastward to margin facies of the Montagna degli Angeli Limestone and to slope and basin deposits of the Mattinata and Maiolica formations, respectively (Bosellini *et al.*, 1999a).

The SGRL is a 500 to 600 m thick, shallow-water carbonate succession spanning the upper Valanginian *p.p.* – Aptian *p.p.* Claps *et al.* (1996) divided this unit into three members, namely members 1 to 3, from the base to the top (Fig. 2). Member 1 (140 m thick) consists of a non-cyclic subtidal succession of mudstone–wackestones and scattered skeletal or oolitic packstone–grainstones. Member 2 (*ca* 310 m thick), is a cyclic succession of ‘loferitic’ beds with layers of green shales and stromatolites, commonly with dinosaur footprints on the bed surfaces (Petti *et al.*, 2008). Member 3 (*ca* 100 m thick) contains a variety of facies, ranging from subtidal high-energy thin-bedded calcarenites to domal stromatolites. The present study focuses on the upper Barremian *p.p.* – lower Aptian *Chondrodonta* accumulations which mark the base of member 3 and crop out in lagoon to tidal flat settings (Posenato *et al.*, 2018).

METHODS

The following methods have been integrated to define the precise stratigraphic position and the ecological significance of the lower Aptian *Chondrodonta* accumulations on the ACP. The stratigraphic framework around the *Chondrodonta* beds was built using biostratigraphic and chemostratigraphic ($\delta^{13}\text{C}$ and $^{87}\text{Sr}/^{86}\text{Sr}$) data. Sedimentological and petrographic analyses were coupled with spectral gamma ray measurements and trace element concentrations to infer early Aptian palaeoenvironmental changes associated with the proliferation of *Chondrodonta*.

Fieldwork and lithofacies analysis

Well-exposed outcrops along road-cuts (Fig. 1B and C) were used to measure two stratigraphic sections. Seven polished slabs of *Chondrodonta*-bearing samples were studied for sedimentological analyses. One hundred and seventy-six thin sections, integrated with outcrop observations, were used for microfacies and biostratigraphic analyses.

Textures were classified based on Dunham (1962), Embry & Klovan (1971), Insalaco (1998)

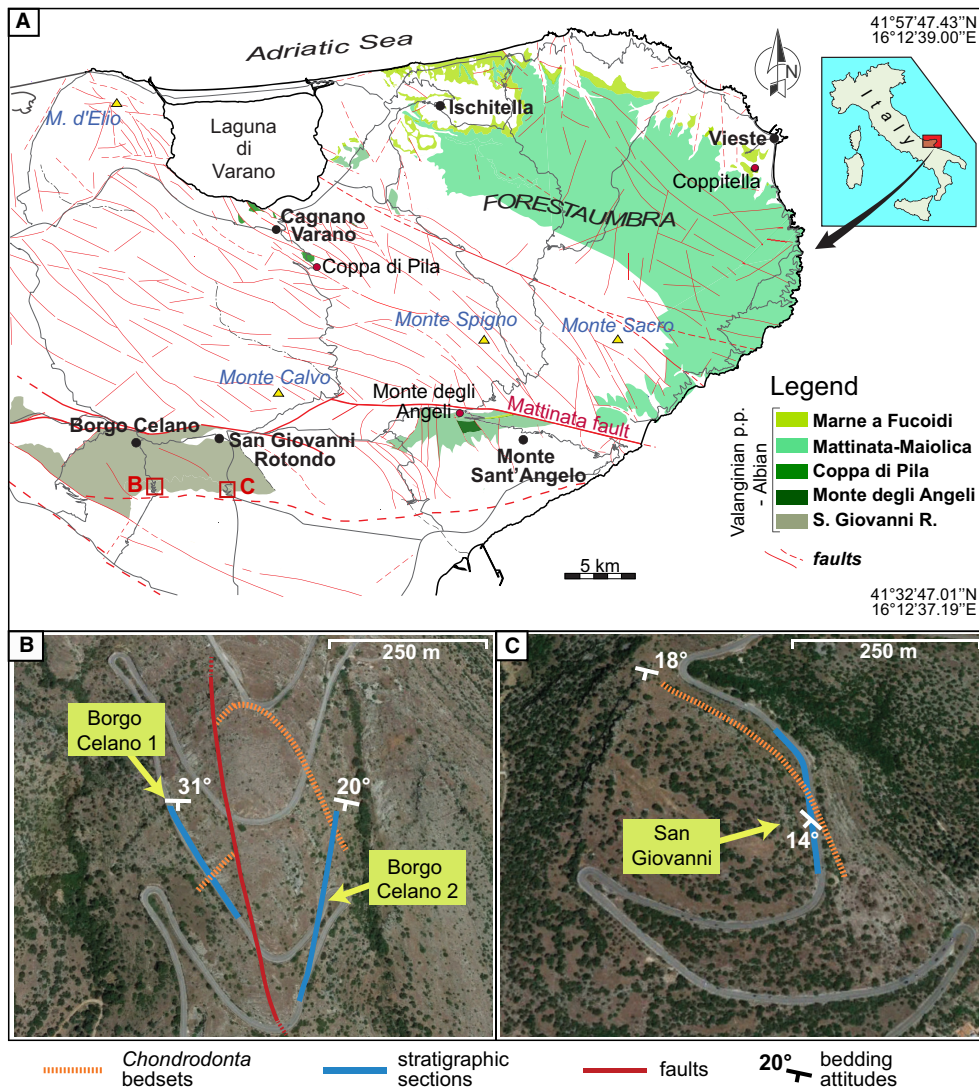


Fig. 1. (A) Simplified geological map of the Gargano Promontory (modified after Morsilli *et al.*, 2017) with location of the studied sections (Borgo Celano and San Giovanni). (B) Location of the two stratigraphic sections in the Borgo Celano area, sampled on opposite sides of the hill following the bedding dip of the *Chondrodonta* bedset. (C) Location of the stratigraphic section in the San Giovanni Rotondo area. Orange dotted lines indicate the position of the *Chondrodonta* bedsets according to the bedding dip measurements.

and Lokier & Al Junaibi (2016). Depositional textures for lithofacies definition were analysed semi-quantitatively and expressed in terms of relative abundance. The biostratigraphic schemes proposed in Claps *et al.* (1996) for the SGRL were updated based on more recent reviews of dasycladales (Carras *et al.*, 2006) and of benthic foraminifera (Velić, 2007; Schröder *et al.*, 2010; Chiocchini *et al.*, 2012).

The *Chondrodonta* accumulations are here defined as ‘bedsets’ (Campbell, 1967) because they are composed of superimposed levels

forming a unique set of *Chondrodonta* beds, about or more than 1 m thick and laterally continuous (see Posenato *et al.*, 2018, for the detailed taphonomic description).

The classification of oligotrophic, mesotrophic and eutrophic associations is based on the nutrient gradients in modern low latitude waters reported in milligrams of chlorophyll α per cubic metre of seawater (see fig. 2 in Mutti & Hallock, 2003) and estimated for the Lower Cretaceous dominant benthos (see fig. 10 in Rameil *et al.*, 2010). Rudist limestones are here considered

	not exposed	
Aptian	San Giovanni Rotondo Limestone	member 3 100 m-thick
Barremian		member 2 310 m-thick
Hauterivian		member 1 140 m-thick
Valanginian	Sannicandro Limestone	
Berriasian		
Mid.-Late Jur.		

Fig. 2. Lithostratigraphic framework proposed for the inner platform carbonates of the Lower Cretaceous San Giovanni Rotondo Limestones (Claps *et al.*, 1996).

indicative of oligotrophic to mesotrophic conditions and the replacement of rudists by mesotrophic taxa like orbitolinids and *Bacinella–Lithocodium* is considered indicative of elevated nutrient levels (Vilas *et al.*, 1995; Huck *et al.*, 2010; Rameil *et al.*, 2010; Najarro *et al.*, 2011; Núñez-Useche *et al.*, 2020). Spectral gamma-ray measurements were made with a hand-held spectrometer (Radiation Solutions model RS-125) to measure relative variations in the concentration of organic matter in the bulk rocks.

Geochemical methods

A total of 140 samples were analysed for $\delta^{13}\text{C}$ and $\delta^{18}\text{O}$ ratios within the micritic portion of the rock matrix. The polished slabs were studied under a binocular microscope and checked with the respective thin sections to identify areas free from large bioclasts or recrystallization. Some samples underwent duplicate analyses to assess reproducibility within a given sample but across potential variation in microfabric. All results are reported in per mil (‰), in the conventional δ notation with reference to the Vienna Pee Dee Belemnite (VPDB) standard.

Fourteen samples from the San Giovanni section were analysed for the elemental concentration through Laser Ablation – Inductively Coupled Plasma – Mass Spectrometry (LA-ICP-MS). The purest micritic fraction of all samples was chosen

to measure the concentration of phosphorous and of a selected group of Redox-Sensitive Trace Elements (RSTE) comprehensive of vanadium, arsenic, molybdenum and uranium. Results were normalized to the concentration of aluminum (Al) on the assumption that Al represents the clay mineral detrital input (e.g. Pearce *et al.*, 2009; Westermann *et al.*, 2013; Hueter *et al.*, 2019).

A total of 12 shell fragments of *Chondrodonta* and rudists was measured for $^{87}\text{Sr}/^{86}\text{Sr}$ chemostratigraphy. To assess the preservation of the original microstructure, shells were screened petrographically using visible light and, where possible, analysed for elemental concentration of magnesium, strontium, manganese and iron (see Brand & Veizer, 1980; Steuber *et al.*, 2005; Frijia *et al.*, 2015). The numerical ages were then translated into the chronostratigraphic ages of the GTS2012 (McArthur *et al.*, 2012). For details on the geochemical methods, see the Supporting Information section.

RESULTS

Lithofacies and lithofacies associations

Based on sedimentological and petrographic analyses of outcrops and thin sections, eleven lithofacies were identified (Table 1, Fig. 3). Textures change from mud to grain-supported to even bindstones; the benthic fauna is mainly represented by bivalves (requieniids and *Chondrodonta*), foraminifera and dasycladales. Micro-encrusts (for example, *Bacinella–Lithocodium*) are particularly concentrated in some stratigraphic intervals. The eleven lithofacies were grouped into three lithofacies associations (LA) (Table 1) and interpreted in terms of depositional environment.

Lithofacies association 1 (LA1) consists of mud-supported and bioturbated bioclastic wackestone (BW) and bioturbated mudstone (MD) facies episodically interbedded with beds of PP and BF (Fig. 3). Microbialites form both stromatolitic bindstones (ST) and discontinuous laminar microstructures in MD, BW and peloidal-bioclastic packstone (PP). *Chondrodonta* boundstones (CH) also occur. The benthic fauna is composed by scattered bivalves (for example, requieniids and *Chondrodonta*) and by common micro-encrusts like *Thaumatoporella* and *Cayeuxia*. This mud-dominated lithofacies association is interpreted to have been deposited in low-energy protected subtidal settings with a mostly restricted marine

Table 1. Summary of the main sedimentological characters of the lithofacies associations and of the 11 lithofacies recognized in the studied sections. Components considered are, in order; skeletal, micro-encrusters and non-skeletal grains. Their relative abundance is expressed as: *a*, abundant, *c*, common, *r*, rare. Laminar and patchy cloudy shapes of *Bacinella–Lithocodium* bindstones are from Huck *et al.* (2010).

Lithofacies	Textures	Bed features and thickness	Components	Sedimentary and diagenetic features	Lithofacies association and depositional settings
MD - Bioturbated mudstone	Mudstone; mudstone–wackestone	Massive and tabular centimetre to metre-thick beds	<i>Chondrodonta</i> and requieniid fragments (r), dasycladales (r), foraminifera (r), small-sized oncoids (r), solitary corals (r), echinoderm spines (r); <i>Thaumatoporella</i> (c-r), <i>Cayeuxia talli</i> (r); peloids (c-r)	Bioturbation, burrows, discontinuous microbial laminae, peloidal-grainstone pockets	LA1 Low-energy protected lagoon passing to tidal flat
BW - Bioclastic wackestone	Wackestone	Massive and tabular centimetre to metre-thick beds	Foraminifera (a-c), <i>Salpingoporella</i> sp. (a-c), small-sized oncoids (c-r), solitary corals and echinoderm spines (r), bivalve and gastropod fragments (r), ostracods (r); <i>Thaumatoporella</i> (c); peloids (c-r)	Peloidal-grainstone pockets, bioturbation, discontinuous microbial laminae	LA1
PP – Peloidal–bioclastic packstone	Packstone–wackestone	Tabular and thin-layered decimetre to metre-thick beds	Foraminifera (c-r), ostracods (a-r), dasycladales (r), bivalve fragments (r), solitary corals and echinoderm spines (r); <i>Thaumatoporella</i> (c-r); peloids (a)	Horizontal shell layers, rare discontinuous microbial laminae	LA1
BF - Bivalve floatstone	Floatstone; mudstone–wackestone matrix	Massive and tabular decimetre to metre-thick beds	Requieniids (a), <i>Chondrodonta</i> (c), nerineids (c-r), oncoids (c-r), foraminifera (c-r), <i>Salpingoporella</i> sp. (c-r), solitary corals and echinoderm spines (r); <i>Thaumatoporella</i> (a-r); peloids (c-r)	Breakage of shells, rare micro-encrustations	LA1
ST - Stromatolite	Bindstone	Tabular to domal decimetre to metre-thick beds or centimetre-thick layers within mud facies	Ostracods (r), bivalve fragments (r), foraminifera (r); <i>Thaumatoporella</i> (c), microbialitic laminae (a); peloids (a-c)	Planar, wavy, dome-shaped laminae	LA1

Table 1. (continued)

Lithofacies	Textures	Bed features and thickness	Components	Sedimentary and diagenetic features	Lithofacies association and depositional settings
CH - <i>Chondrodonta</i> boundstone	Boundstone; mudstone–wackestone or wackestone–packstone matrix	Tabular and nodular decimetre-thick beds forming a unique bedset; shells both horizontally oriented (i.e. toppled) or in life-position	<i>Chondrodonta</i> (a), requieniids (r), foraminifera (r), dasycladales (r); <i>Thaumatoporella</i> (r), <i>Cayeuxia talli</i> (c-r), microbial crusts (c-r); peloids (r)	Horizontal shell layers, microbial crusts	LA1
PG – Peloidal–foraminiferal packstone–grainstone	Packstone–grainstone; grainstone	Thin-layered centimetre to decimetre-thick beds	Foraminifera (a-c), <i>Salpingoporella</i> sp. (c), small-sized oncoids (c-r), undetermined bivalve fragments (c-r), echinoderm spines (r); <i>Thaumatoporella</i> (c-r); peloids (a), mudclasts (c), aggregate grains (r)	Micritization, micro-encrustations	LA2 High-energy open lagoon
RF – Bivalve floatstone–rudstone	Floatstone–rudstone; packstone–grainstone matrix	Massive, tabular, and occasionally lens-shaped centimetre to metre-thick beds	Requieniids (a-c), <i>Chondrodonta</i> (c), nerineids (c), oncoids (c), foraminifera (a-c), dasycladales (c-r), undetermined bivalve fragments (c-r), echinoderm spines (c-r), solitary corals (r); <i>Thaumatoporella</i> (r), peloids (a-c), mudclasts (c-r), ooid fragments (r)	Bioerosion, bivalve lenses, breakage of shells, micritization, micro-encrustations	LA2
OF – Oncoid floatstone–rudstone	Floatstone–rudstone; packstone–grainstone matrix	Massive and tabular decimetre to metre-thick beds	Oncoids (a), nerineids (a-c), foraminifera (a-c), dasycladales (c-r), undetermined bivalve fragments (c-r), solitary corals (r), echinoderm spines (r); <i>Thaumatoporella</i> (c-r), <i>Cayeuxia talli</i> (r); peloids (a-c), ooids (r), mudclasts (r), aggregate grains (r)	Micritization, micro-encrustations	LA2

Table 1. (continued)

Lithofacies	Textures	Bed features and thickness	Components	Sedimentary and diagenetic features	Lithofacies association and depositional settings
LB – Floatstone–rudstone with common <i>Bacinella</i> – <i>Lithocodium</i>	Floatstone–rudstone; packstone–grainstone or wackestone matrix	Tabular decimetre-thick beds	Requieniids (a-c), oncoids (a-c), nerineids (c-r), <i>Chondrodonta</i> (c-r), solitary corals (c-r), echinoderm spines (r); foraminifera (c), dasycladales (c-r); <i>Thaumatoporella</i> (r), <i>Bacinella</i> – <i>Lithocodium</i> (c), <i>Cayeuxia talli</i> (r); peloids (a), mudclasts (c-r), aggregate grains (r)	Micro-encrustations	LA3 Moderate-energy lagoon under stressed conditions
BL – <i>Bacinella</i> – <i>Lithocodium</i> bindstone	Bindstone	Centimetre to decimetre-thick nodular beds	Undetermined bivalve fragments (c-r), foraminifera (r), echinoderm spines (r), solitary corals (r), small-sized oncoids (r); <i>Thaumatoporella</i> (r), <i>Bacinella</i> – <i>Lithocodium</i> (a); peloids (c-r)	Laminar to patchy cloudy micro-encrustations	LA3

circulation, as indicated by the poorly differentiated biotic assemblages. Inter-supratidal facies and sedimentary structures (i.e. stromatolite lithofacies – ST – fenestrae and exposure surfaces) indicate occasional shifts to tidal-flat settings. Subtidal cycles prevail whereas peritidal cycles, capped by stromatolites or by exposure surfaces, are less common. Apart from the singular occurrence of CH, all lithofacies of LA1 are typical of inner platform settings documented in many adjacent Tethyan carbonate platforms (e.g. Husinec & Read, 2011, 2018; Di Lucia *et al.*, 2012; Amodio & Weissert, 2017, among others).

Lithofacies association 2 (LA2) consists of grain-supported facies [peloidal–foraminiferal packstone–grainstone (PG), bivalve floatstone–rudstone (RF) and oncoïd floatstone–rudstone (OF)] with high skeletal content and diversity (Fig. 3). The benthic fauna is composed of common to abundant bivalves (requieniids and *Chondrodonta*), nerineid gastropods, foraminifera and dasycladales. Based on textures and skeletal components, as well on the absence of exposure surfaces or inter-supratidal sedimentary structures (common in LA1), LA2 can be interpreted as deposited in a typical subtidal

environment or protected lagoon. The latter is characterized by a more open circulation with episodic high-energy events (PG and OF) and by short-term transgressive phases during the accumulation of RF. A similar interpretation of this type of lithofacies has been given in other inner platform settings (e.g. Husinec & Read, 2018).

Lithofacies association 3 (LA3) is based on the occurrence of *Bacinella*–*Lithocodium* both as bindstones (BL) and as micro-encrustations in floatstone–rudstones (LB) (Fig. 3). These micro-encrustations are concentrated in specific intervals of the stratigraphic succession, in which they predominate over other biota. BL and LB facies alternate with LA2 grain-supported lagoon facies and, less commonly, with mud-supported beds of LA1. *Bacinella*–*Lithocodium* facies have been considered as indicative of environmental stress on the platform top (Immenhauser *et al.*, 2005). LA3 can be therefore interpreted as deposited in moderate-energy lagoon settings under environmentally stressed conditions. In other lower Aptian shallow-water platforms (for example, Arabian and Adriatic Carbonate Platforms) the occurrence of these micro-encrustations, also in the form of small patchy bioherms, is associated with the

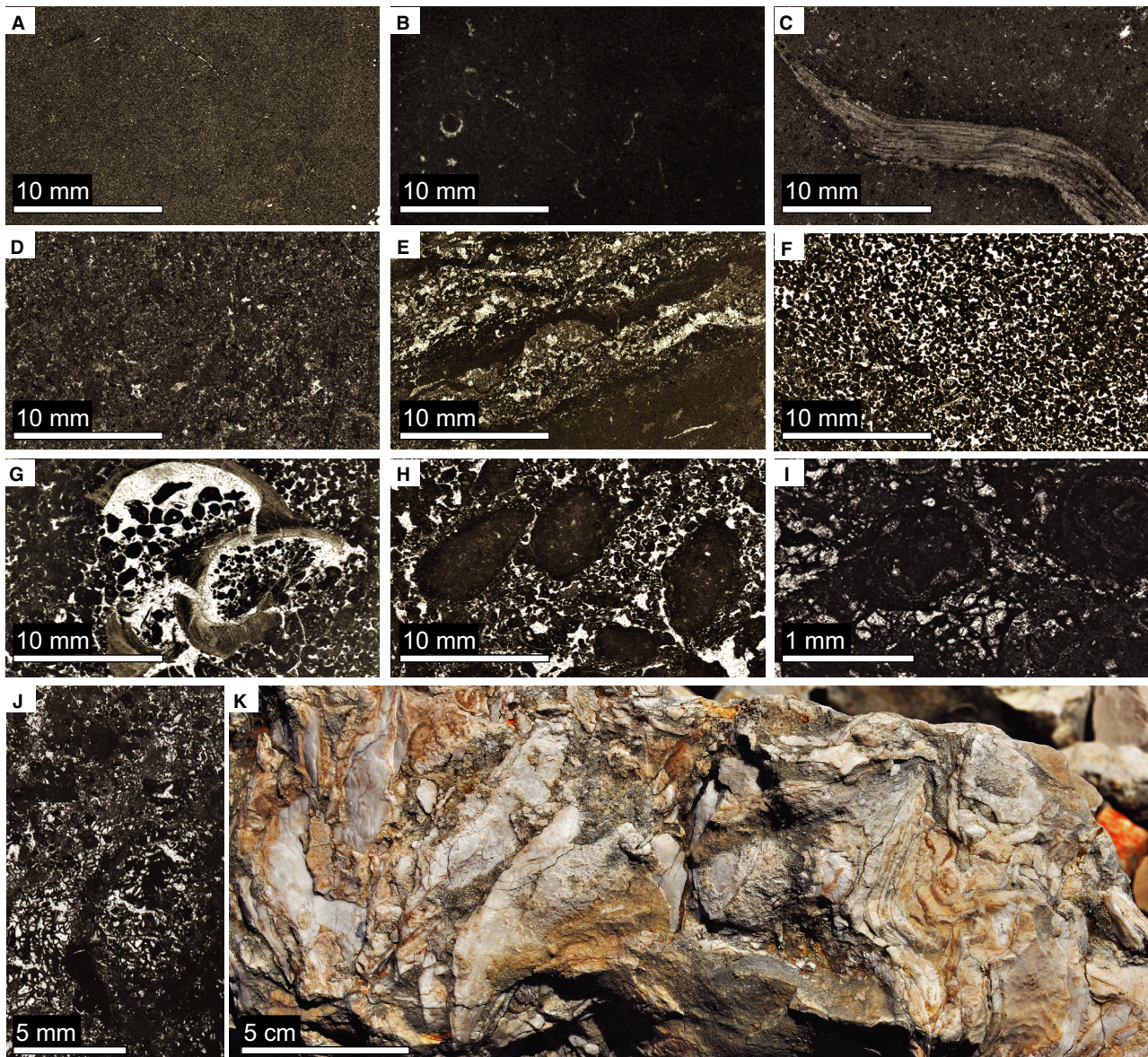


Fig. 3. Photographs of the eleven lithofacies with the main characteristics recognized in the investigated sections. (A) Bioturbated mudstone (MD). (B) Bioclastic wackestone (BW). (C) Bivalve floatstone (BF). (D) Peloidal-bioclastic wackestone-packstone (PP). (E) Stromatolite (ST). (F) Peloidal-foraminiferal packstone-grainstone (PG). (G) Bivalve floatstone-rudstone (RF). (H) Oncoid floatstone-rudstone (OF). (I) Floatstone-rudstone with common *Bacinella-Lithocodium* (LB). (J) *Bacinella-Lithocodium* bindstone (BL). (K) *Chondrodonta* boundstone (CH), bouquet-like shell aggregates from the upper part of the *Chondrodonta* bedset in the Borgo Celano area.

environmental instability related to OAE1a (e.g. Immenhauser *et al.*, 2005; Huck *et al.*, 2010; Rameil *et al.*, 2010; Hueter *et al.*, 2019).

Stratigraphy and geochemical results

The San Giovanni section

The San Giovanni stratigraphic section (Figs 1C and 4) is 23.8 m thick and records low-skeletal,

mud-supported facies gradually passing to grain-supported rudist beds with *Bacinella-Lithocodium* micro-encrustations. The lower part (0 to 15.9 m, SGRL, uppermost member 2 to lowermost member 3) is mostly composed of LA1 metre-thick massive mudstones (MD), miliolid-algal wackestones (BW) and peloidal packstones – locally wackestones (PP). Microbial activity generates both decimetre-thick tabular and

domal stromatolites (ST) and discontinuous peloidal – microbial laminae in MD, BW and PP. All of these beds are abundantly bioturbated and show common ephemeral emersion-related features like breccias, vugs and fenestrae. Less common LA2 thin-bedded peloidal packstone–grainstones (PG) and oncoid floatstone–rudstones (OF) are intercalated and gradually increase upward in thickness and frequency. *Chondrodonta* and nerineids, oncoids, miliolids and micro-encrusters (for example, *Cayeuxia* and *Thaumatoporella*) are common; ostracods are locally abundant and horizontally oriented in thin layers (4.0 to 5.4 m). The *Chondrodonta* bedset (base of member 3, CH and locally BF) occurs between 7.1 m and 9.25 m, on top of a tabular stromatolite, and is overlain by BW, PP and OF beds rich in oncoids and *Thaumatoporella* and barren in molluscs, foraminifera and dasycladales (10.0 to 13.5 m). The uppermost occurrence of *Salpingoporella muehlbergii* is at the base of the section and the micro-component association of *Cuneolina* sp., *Debarina* sp., *Praechrysalidina infracretacea*, *Pseudolituonella* sp. and *Salpingoporella* sp. occurs above the *Chondrodonta* bedset (ca 10 m from the base).

The upper part of the section (15.9 to 23.8 m, SGRL, member 3) lacks stromatolites and is mainly composed of LA2 and LA3 facies. The base of the section is a metre-thick peloidal–packstone (PP) overlain by thin-bedded peloidal–foraminiferal packstone–grainstones (PG) interbedded with centimetre-thick requieniid beds (RF) and metre-thick oncoid floatstone–rudstones (OF). Requiieniids increase upward in size and abundance and are locally arranged in lenticular accumulations. *Chondrodonta* occurs as common bioclasts with nerineids, dasycladales (*Salpingoporella* sp.) and foraminifera (miliolids, *P. infracretacea* and *Cuneolina* sp.); orbitolinids are scattered within requieniid facies (17.5 to 21.0 m from the base). *Bacinella–Lithocodium* micro-encrustations (LB) occur commonly across the upper part of the section; a *Bacinella*-bindstone (BL) occurs between 18.5 m and 19.3 m in association with requieniid fragments and orbitolinids. The first occurrence of *Salpingoporella dinarica* is at 18.5 m above the base.

The $\delta^{13}\text{C}$ curve in the San Giovanni section (Fig. 4) records an overall upward decreasing trend from +0.1‰ to –1.1‰ and a range of values between +0.7‰ and –4.8‰, with a mean of –1.3‰. Above the *Chondrodonta* bedset, a sharp

negative shift from –0.6‰ to –2.4‰ (9.8 to 10.1 m) marks the onset of a negative plateau that extends up to 15.9 m and contains the most negative values of the entire $\delta^{13}\text{C}$ curve. The overall decreasing trend in $\delta^{18}\text{O}$ is less marked and does not show abrupt positive or negative shifts; $\delta^{18}\text{O}$ values decrease from –2.7‰ to –4.6‰, with an average of –3.9‰.

The concentration of Al in the San Giovanni section averages around 500 ppm and shows a sharp positive peak of 3000 ppm right above the *Chondrodonta* bedset (ca 10 m), in correspondence of an oncoid–floatstone with ephemeral emersion-related features (Fig. 5). The P/Al ratio averages around 0.1, with a weak increase within the *Chondrodonta* bedset, followed by a sharp decrease immediately above it.

The Redox-Sensitive Trace Elements (RSTE)/Al ratios show generally low values. Within the *Chondrodonta* bedset, both the V/Al and the Mo/Al ratios show short fluctuations, between 0.01 and 0.02 and between 0.001 and 0.002, respectively. The As/Al and the U/Al ratios show sharper positive peaks, up to 0.003 and up to 0.01, respectively. At the top of the bedset, all of the RSTE/Al values abruptly decrease, and their curves flatten.

In the uppermost part of the section (ca 11.5 m), both the P/Al and the RSTE/Al ratios culminate in positive peaks at an exposure surface.

The Borgo Celano 1 section

The Borgo Celano 1 stratigraphic section (Figs 1B and 6A) is 25.3 m thick (SGRL, members 2 and 3) and consists of lime mud-rich beds interbedded with grain-supported and bioclastic deposits. *Bacinella–Lithocodium* micro-encrustations occur in the uppermost part of the section.

Most of the section consists of alternating LA1 and LA2 facies associations with rare LA3. The lowermost 13.5 m are characterized by metre-thick and decimetre-thick foralgal–*Thaumatoporella* wackestones (BW), bioturbated mudstones (MD) and molluscan floatstones with common *Chondrodonta*, requieniids and nerineids (BF). These lithofacies are intercalated with decimetre-thick, thin-bedded peloidal–foraminiferal packstones and grainstones (PP and PG) and bioclastic–oncoid rudstones and floatstones (OF and RF). The abundance of skeletal material is moderate, especially for foraminifera and dasycladales; ostracods are locally common and micro-encrusters, except for scattered *Thaumatoporella*, are rare.

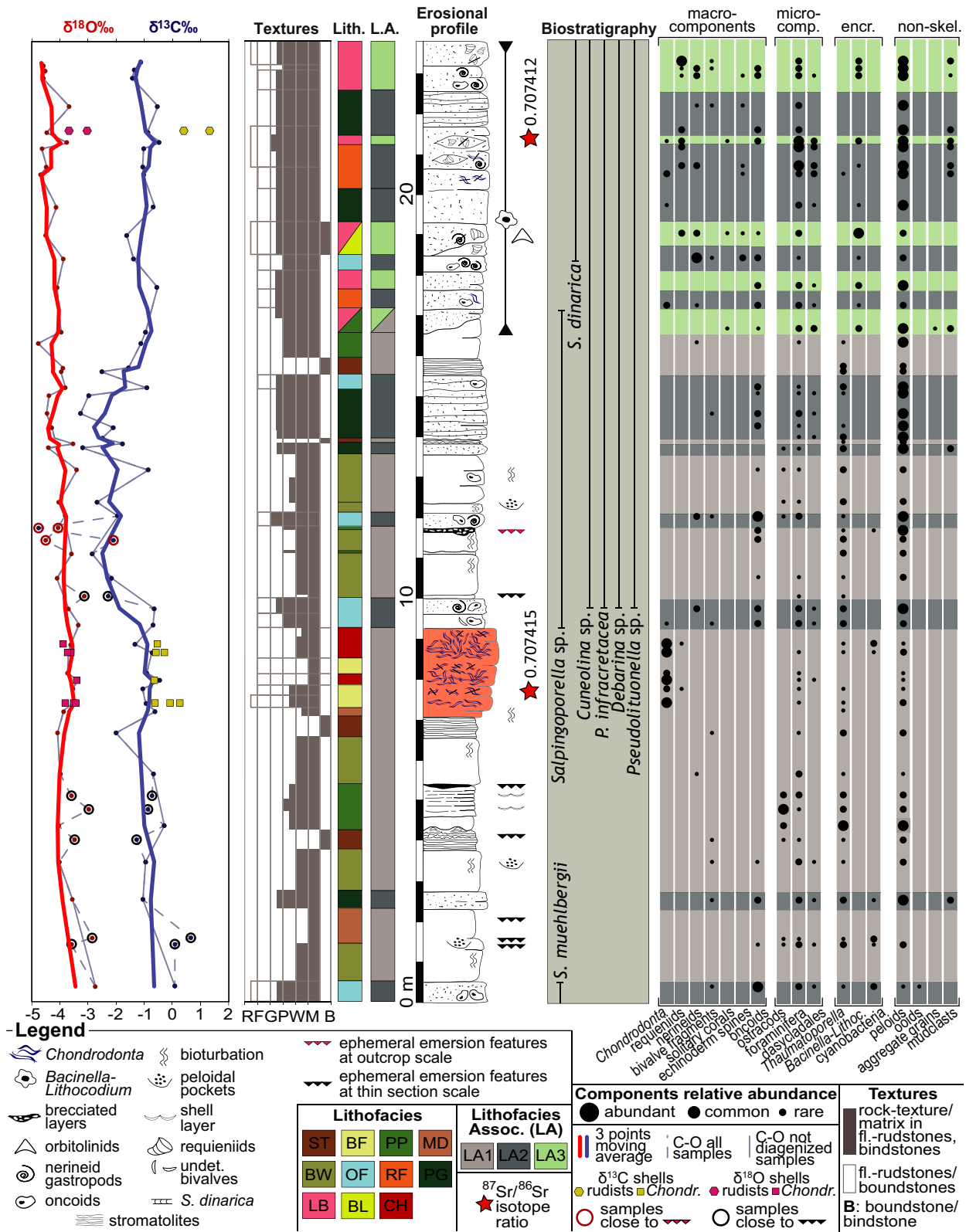


Fig. 4. San Giovanni stratigraphic log (base: 41°40'19.90"N, 15°43'44.30"E; top: 41°40'13.85"N, 15°43'46.05"E) including biostratigraphy and stable isotope results ($\delta^{18}\text{O}$, $\delta^{13}\text{C}$, $^{87}\text{Sr}/^{86}\text{Sr}$). Rock-components are analysed semi-quantitatively and their abundance is expressed relative to the rock texture. The *Chondrodonta* bedset is highlighted in orange; see text and Table 1 for the description of lithofacies and lithofacies associations.

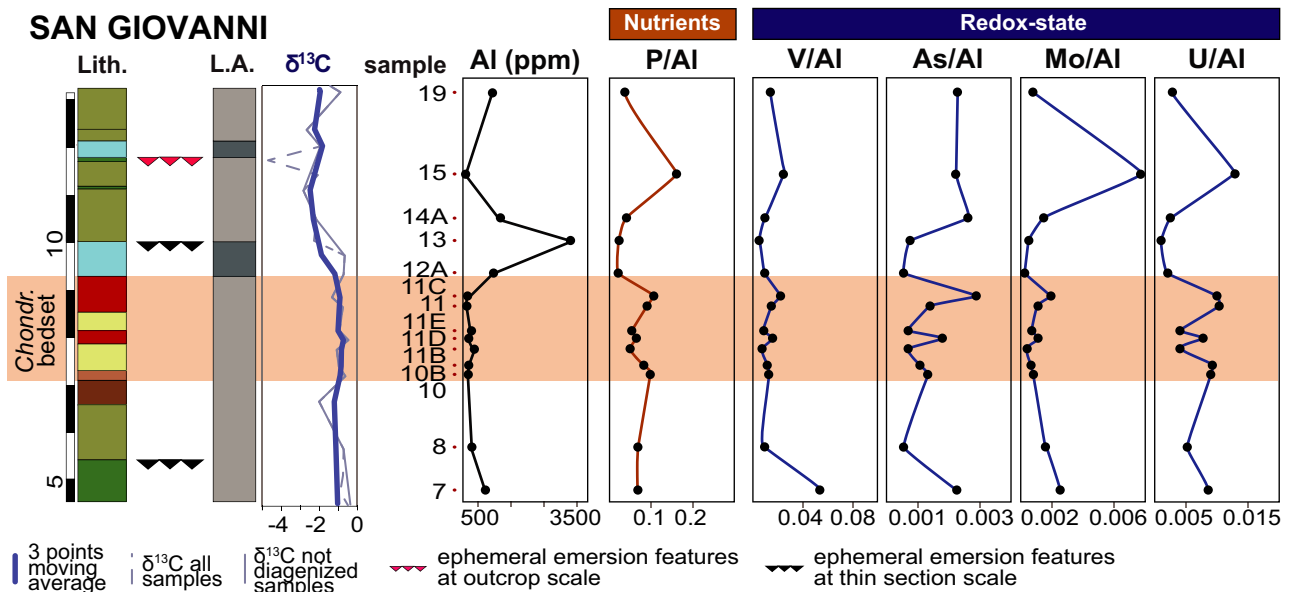


Fig. 5. Trace element concentrations in the lower part of the San Giovanni section (4.7 to 13.1 m), including aluminium (Al) as terrigenous input proxy, phosphorous (P) as nutrient proxy and a set of Redox-Sensitive Trace Elements (V, As, Mo and U). P and RSTÉ values are normalized on the concentration of aluminium (see Supporting Information for details) and reported as element/Al ratios.

Higher in the section (13.5 to 22.5 m) the bioclastic content, especially requieniids, decreases gradually. Microbial activity generates discontinuous microbial-peloidal laminae in MD and BW as well as decimetre-thick domal and tabular stromatolites (ST), interlayered with mudstones and grain-supported facies. Ephemeral emersion-related features like vugs and fenestrae are common. The *Chondrodonta* bedset (15.5 to 16.1 m, SGRL, base of member 3, CH and locally BF) overlies a tabular stromatolite and is followed by *ca* 3 m of limestones depleted in molluscs, foraminifera and dasycladales, and relatively enriched in *Thaumtoporella* and other micro-encrusters (for example, *Cayeuxia thalli*). The last occurrence of *S. muehlbergii* is recorded 11 m above the base of the section. *Cuneolina* sp., *P. infracretacea*, *Nezzazzatids*, *Debarina* sp. and *Pseudolituonella* sp. gradually appear upward; *Mayncina* sp., *Salpingoporella heraldica* and *Actinoporella podalica* occur around the *Chondrodonta* bedset.

The uppermost part of the section (22.5 to 25.3 m) consists of LA2 and LA3 facies associations and starts with a massive peloidal packstone-grainstone (PG) rich in foraminifera (miliolids, *Cuneolina* sp. and *P. infracretacea*) and dasycladales (*Salpingoporella* sp.). It is

followed by oncoid floatstone-rudstone beds (OF) and bivalve (requieniids and *Chondrodonta*) floatstones with scattered orbitolinids and common *Bacinella-Lithocodium* micro-encrustations (LB).

The $\delta^{13}\text{C}$ curve in the Borgo Celano 1 section (Fig. 6B) records an overall slightly upward increasing trend from -2.1‰ at the base to -0.9‰ at the top, with a mean of -0.9‰ . In the lower part of the section, the positive trend is punctuated at 11 m by a negative shift from $+0.1\text{‰}$ (the highest value of the $\delta^{13}\text{C}$ curve) to about -3.0‰ . This shift marks the base of a negative plateau occurring up to 18 m, with values averaging around -0.9‰ . The $\delta^{18}\text{O}$ curve exhibits a similar, slightly increasing trend from -4.6‰ at the base to -3.8‰ at the top, with an average of -3.7‰ and no sharp positive or negative shifts.

The total gamma ray intensity is generally below 20.0 API units in the first 13 m of the Borgo Celano 1 section (Fig. 6B). It shows an overall increase up-section, with peaks up to 40.0 (8.0 to 11.5 m) and 50.0 API units (at 19.8 m). The concentration of uranium is lower than 2 ppm in the first 13 m and increases upward with peaks of more than 5 ppm (at 18.4 m and 20 m, respectively). Above 20 m, signals of both total gamma ray and uranium

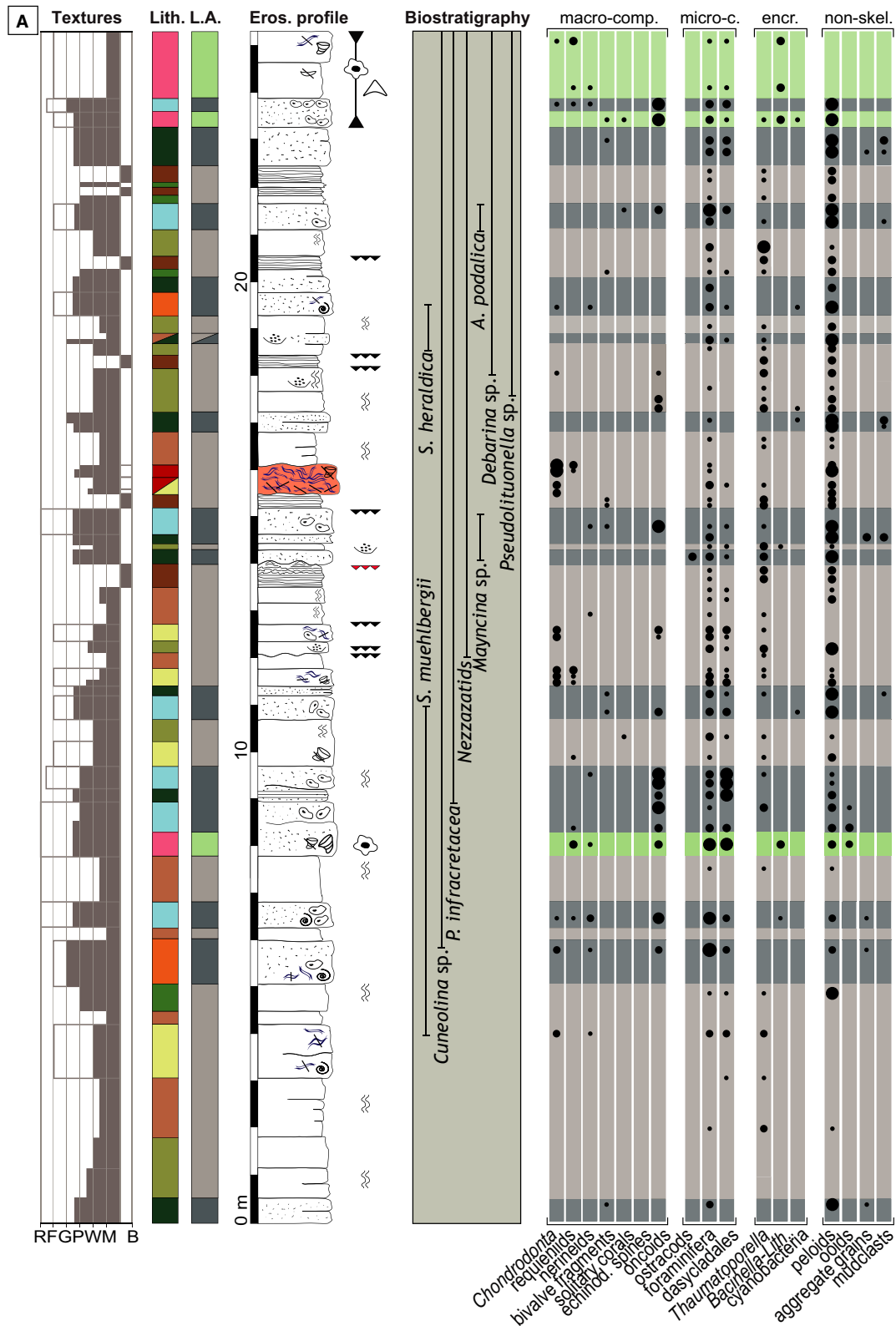


Fig. 6A. Borgo Celano 1 stratigraphic log (base: 41°40′31.38″N, 15°39′58.40″E; top: 41°40′27.35″N, 15°40′01.85″E) including biostratigraphy. Rock-components are analysed semi-quantitatively and their abundance is expressed relative to the rock texture. The *Chondrodonta* bedset is highlighted in orange; see text and Table 1 for the description of lithofacies and lithofacies associations and Fig. 4 for the legend.

B

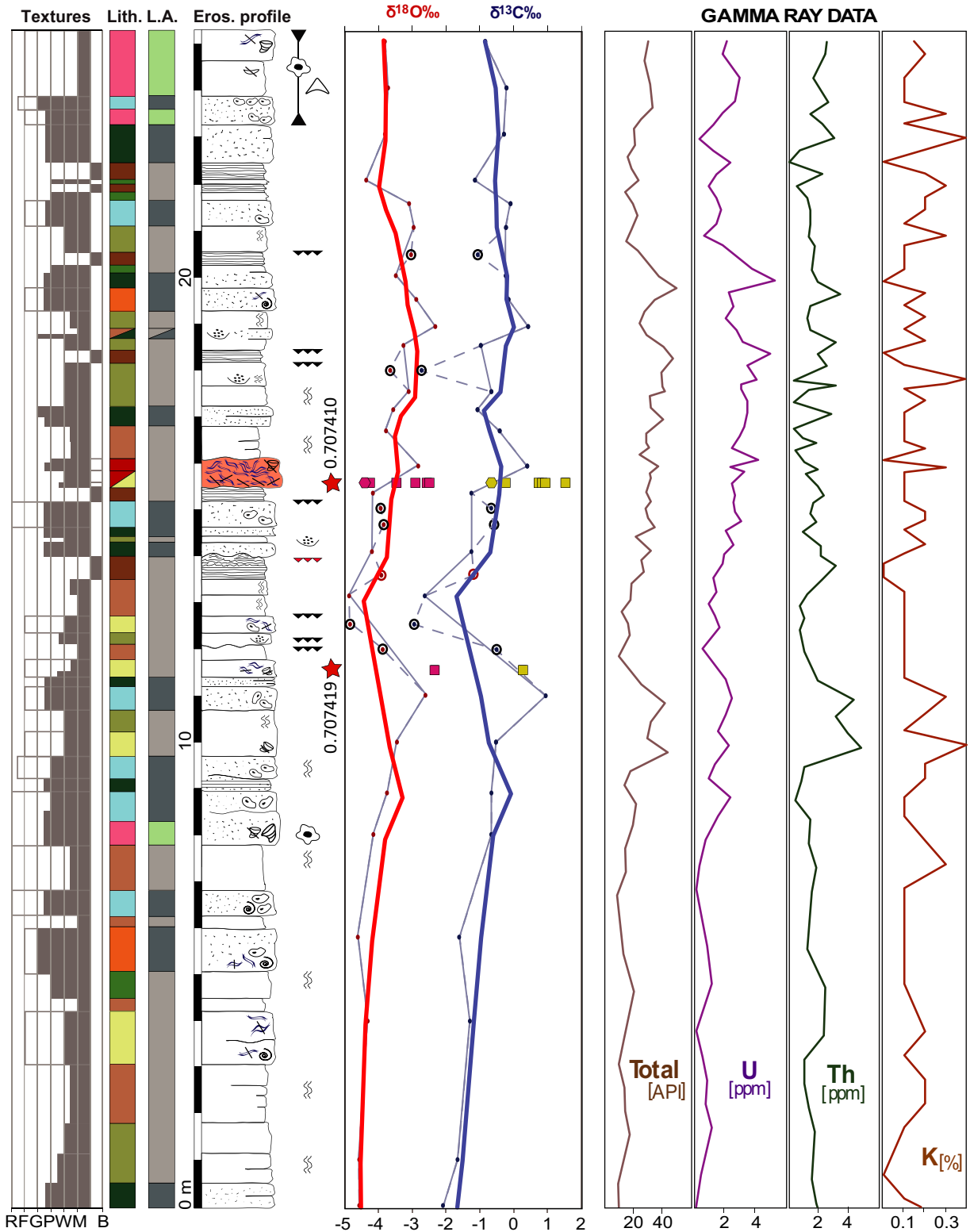


Fig. 6B. Borgo Celano 1 stratigraphic log including stable isotope ($\delta^{18}\text{O}$, $\delta^{13}\text{C}$, $^{87}\text{Sr}/^{86}\text{Sr}$) results and gamma ray data (Total API, uranium, thorium and potassium). The *Chondrodonta* bedset is highlighted in orange; see text and Table 1 for the description of lithofacies and lithofacies associations and Fig. 4 for the legend.

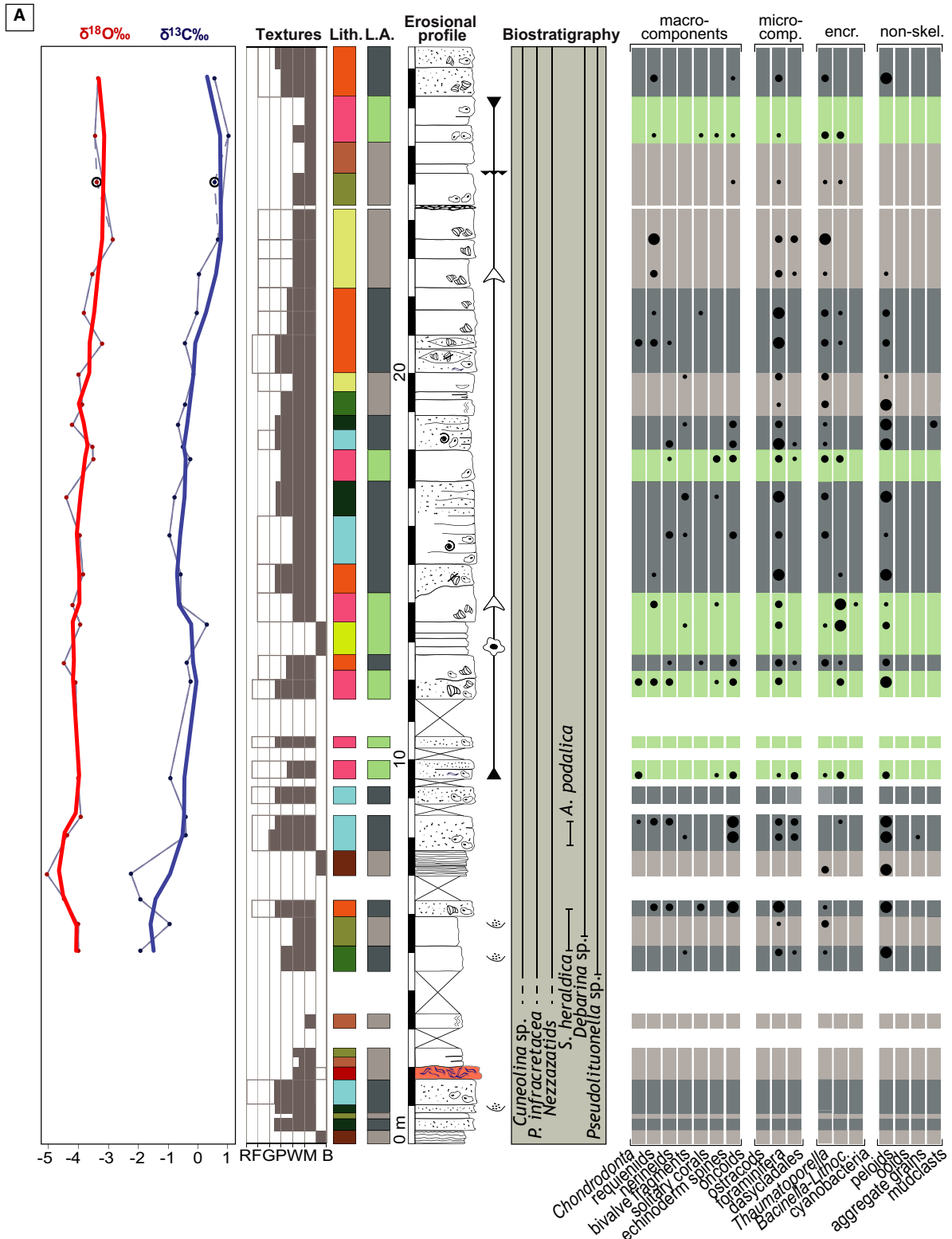


Fig. 7A. Borgo Celano 2 stratigraphic log (lower part) (base: 41°40′31.7″N, 15°40′07.55″E; top: 41°40′24.30″N, 15°40′04.70″E) including biostratigraphy and stable isotope results ($\delta^{18}\text{O}$, $\delta^{13}\text{C}$). Rock-components are analysed semi-quantitatively and their abundance is expressed relative to the rock texture. The *Chondrodonta* bedset is highlighted in orange; see text and Table 1 for the description of lithofacies and lithofacies associations and Fig. 4 for the legend.

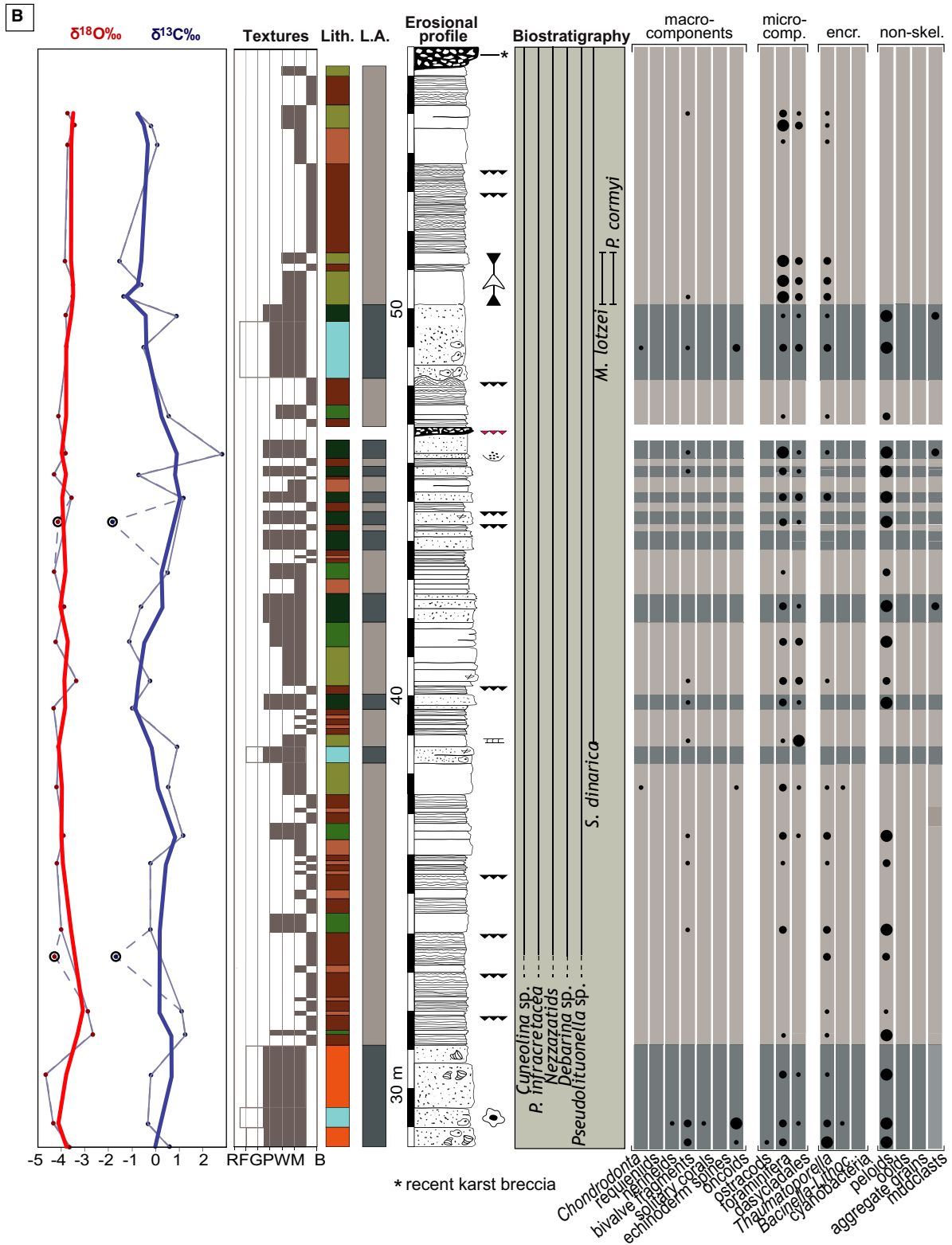


Fig. 7B. Borgo Celano 2 stratigraphic log (upper part) (base: 41°40'31.7"N, 15°40'07.55"E; top: 41°40'24.30"N, 15°40'04.70"E) including biostratigraphy and stable isotope results ($\delta^{18}O$, $\delta^{13}C$). Rock-components are analysed semi-quantitatively and their abundance is expressed relative to the rock texture. The *Chondrodonta* bedset is highlighted in orange; see text and Table 1 for the description of lithofacies and lithofacies associations and Fig. 4 for the legend.

decrease. The concentration of thorium ranges around 2 ppm throughout the section, with peaks of 4 ppm between 8.0 m and 11.5 m. Values decrease to 1 ppm only in the upper part (17 to 20 m from the base). The concentration of potassium varies between 0% and 0.4% throughout the section and shows sharp concentration peaks at 10 m, 17 m and 20 m from the base.

The Borgo Celano 2 section

The Borgo Celano 2 stratigraphic section (Figs 1B, 7A and 7B) is 56.8 m thick (SGRL, member 2 and 3) and shows lime mud-rich facies alternating with grain-supported and bioclastic beds. *Bacinella*–*Lithocodium* micro-encrustations are common in the lower-middle part of the section and stromatolites predominate in the upper part.

The lowermost 7.6 m are composed of alternating LA1 and LA2 facies successions, with a generally low skeletal abundance. It is marked at the base and at the top by tabular stromatolites (ST) and contains bioturbated mudstones (MD) and *Thaumatoporella*–wackestones and packstones (BW and PP). These are interbedded with massive decimetre-thick peloidal–foraminiferal packstone–grainstones (PG) and molluscan–oncid floatstone–rudstones (OF and RF) with requieniids and nerineids. The *Chondrodonta* bedset (1.7 to 2.0 m, base of member 3, CH) occurs within both mud-supported and grain-supported facies.

In the middle part of the section (7.6 to 31.1 m) stromatolites are absent and the skeletal abundance generally increases. This part consists mostly of interbedded LA2 and LA3 skeletal-rich facies, arranged in massive decimetre to metre-thick requieniid–oncid floatstone–rudstones, in both granular and muddy matrices (RF, OF and BF). Requieniids increase upward in size and abundance. These skeletal-rich facies are interbedded with thin-bedded peloidal–foraminiferal packstones and grainstones (PG and PP) and, commonly, with lithofacies LB. *Bacinella*–*Lithocodium* micro-encrustations form bindstones (BL) between 9.5 m and 14.3 m. Common constituents of this middle part include requieniids, small benthic foraminifera (miliolids, *P. infractretacea*, *Cuneolina* sp. and *Debarina* sp.) and dasycladales (*Salpingoporella* sp.). *Thaumatoporella* is locally abundant and orbitolinids occur within the rudist and *Bacinella*–*Lithocodium* facies. *Bacinella*–*Lithocodium* micro-encrustations (LB) eventually disappear in favour

of muddy strata (MD and BW) and, up-section, of grain-supported strata (OF and RF).

The upper part of the section (31.1 to 56.8 m) records the complete disappearance of the LA3 facies association and of rudist limestones. It is composed of LA1 facies with interbedded thin LA2 intervals and is characterized by predominant stromatolites (ST). These occur either as centimetre-thick wavy laminae within MD, as tabular decimetre-thick beds alternating with PP, PG, OF and BW, or as tabular and dome-shaped decimetre to metre-thick beds (between 46.1 m and 56.8 m). The abundance of macrofossils, especially requieniids, is generally low in the upper part of the section; exceptions are noted for *S. dinarica*, which reaches its highest concentration between 38.7 m and 38.9 m, and for the occurrence of an orbitolinid-rich wackestone (*Mesorbitolina lotzei* and *Praeorbitolina cornyi*) at 50.0 to 51.5 m.

The $\delta^{13}\text{C}$ values in the Borgo Celano 2 section (Fig. 7A and B) increase up-section, from -1.9‰ at the base to -0.7‰ at the top, with an average of -0.2‰ . The lower part (0 to 7.6 m) contains a negative peak of -2.2‰ (7 m). Values slightly increase in the middle part (7.6 to 31.1 m) and a short negative shift, from $+0.3\text{‰}$ to -0.1‰ , occurs around the *Bacinella*-rich level (12.0 to 15.8 m). In the upper part of the section (31.1 to 56.8 m) two negative peaks, of -1.7‰ and of -1.9‰ , occur respectively at 33.4 m and at 44.6 m, in correspondence with beds with ephemeral-emersion related features. The most positive peak of the stratigraphic section, of $+2.8\text{‰}$, occurs at 46.35 m. The $\delta^{18}\text{O}$ curve also increases up-section, rising from -4.0‰ at the base to -3.5‰ at the top.

Chondrodonta bedsets

The *Chondrodonta* bedsets occur in the lower-middle part of the studied sections (see Fig. 8A to G), interbedded with carbonate mud-rich facies and stromatolites. The bivalves belong to the species *C. glabra* Stanton (Posenato *et al.*, 2018), form parachthonous to autochthonous accumulations and occur in an almost monospecific association with subordinate requieniids: *C. glabra* shells, 8 to 12 cm long on average, are mostly articulated, present a generally low degree of breakage and show a variable orientation and distribution throughout the bedsets. The outer calcite shell layer is preserved whereas the inner aragonitic one is dissolved (see Posenato *et al.*, 2018).

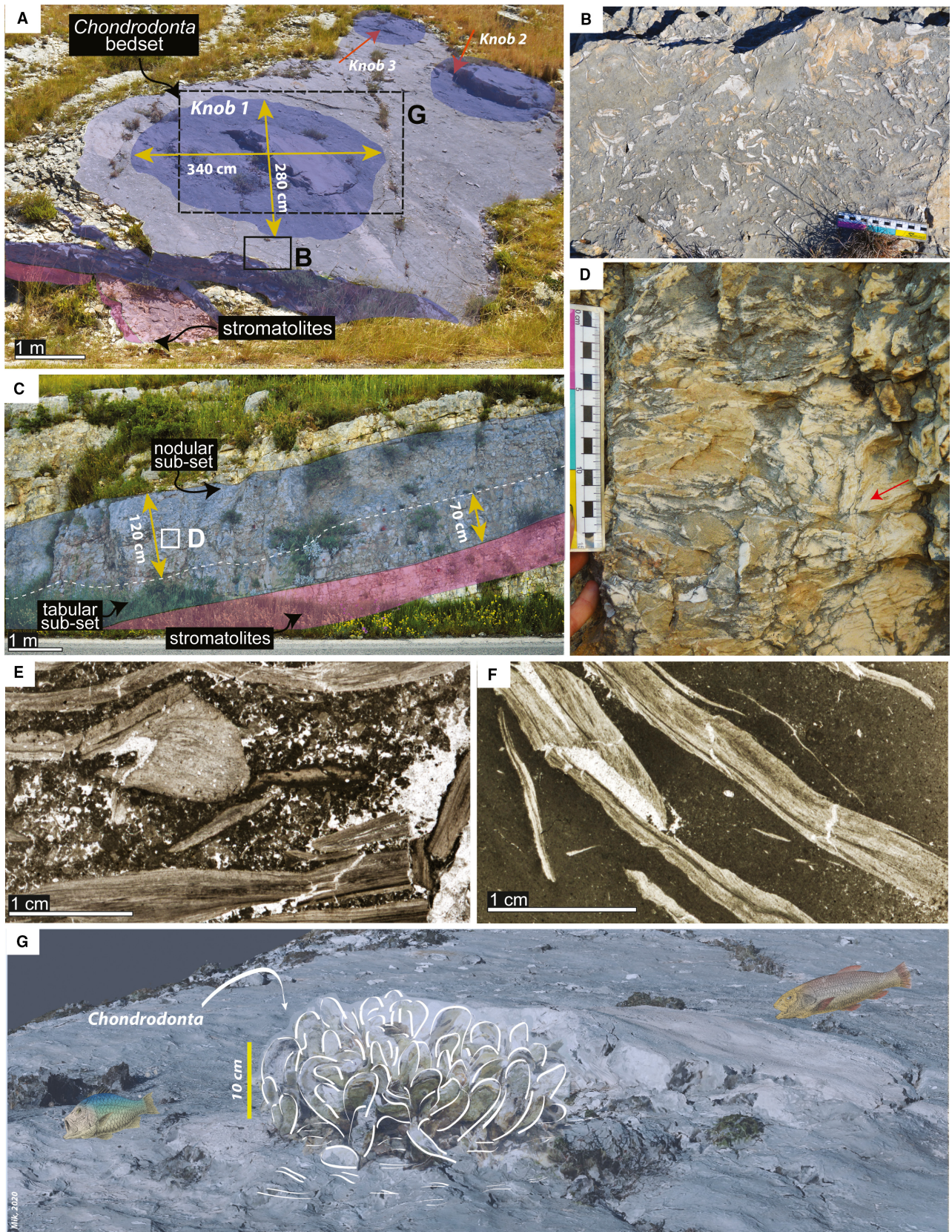


Fig. 8. Field and thin section photographs of the *Chondrodonta* bedsets of the San Giovanni and Borgo Celano 1 sections. (A) Roadcut of the Borgo Celano section, in which the bedset and the underlying stromatolites have been highlighted; red arrows point to two of the three knobby reliefs recognized in Posenato *et al.* (2018). The other relief is marked in darker blue, and its extension is reported in centimetres. (B) Abundant and frequently sub-horizontal shells on the upper surface of the Borgo Celano bedset. (C) Roadcut of the San Giovanni section, in which the bedset and the underlying stromatolites have been highlighted; the bedset has been divided in a lower tabular sub-set, about 60 to 70 cm thick, and an upper nodular subset, 100 to 120 cm thick on average. (D) Close-up of the densely packed sub-horizontal shells in the lower nodular sub-set of the San Giovanni bedset; arrows point to scattered individuals with sub-vertical orientation. (E) and (F) Thin sections from the *Chondrodonta* bedsets, showing: (E) sub-horizontal shells bearing in a *Chondrodonta* fragments-packstone matrix, at Borgo Celano; and (F) sub-vertical shells bearing in a *Chondrodonta* fragments-wackestone matrix, at San Giovanni. Beside *Chondrodonta*, small benthic foraminifera, dasycladales and *Thaumatoporella* are secondary micro-components; microbial crusts are locally around *Chondrodonta* shells at Borgo Celano while *Cayeuxia* is common in the uppermost part of the San Giovanni bedset. (G) Reconstruction of a *Chondrodonta* thicket based on outcrop observations. The used background corresponds to the small knob visible in Fig. 8A.

The *Chondrodonta* bedset in the Borgo Celano 1 section (Fig. 8A) is composed of nodular beds in which chaotically oriented shells and small bouquet-like aggregates (see Fig. 3I) are scattered between dense sheets of sub-horizontal individuals (Fig. 8C). The upper bed surface (Fig. 8A) shows three sub-circular reliefs (*cf.* ‘knobs’; see Posenato *et al.*, 2018) with shells in upright position forming bouquet-like or thicket aggregates (Fig. 8G). In the Borgo Celano 2 section, a few hundred metres eastward, the same *Chondrodonta* bedset is half the thickness and directly overlies subtidal oncoid beds.

In the San Giovanni section, the bedset is composed of two sub-sets (Fig. 8B). The lower sub-set, arranged in decimetre-thick tabular beds, shows locally common *Chondrodonta* in small patches, with sub-horizontal or, less commonly, upright shells. In the upper sub-set, composed of nodular and undulating beds, shells are more abundant and occur either horizontally oriented in dense sheets or chaotically oriented with common bouquet-like aggregates (Fig. 8D).

INTERPRETATION AND DISCUSSION

Reliability of the stable isotope geochemistry

In the last decades, high-resolution $\delta^{13}\text{C}$ stratigraphy has been successfully applied to the correlation of Cretaceous shallow-water platform carbonates and hemi-pelagic deposits (e.g. Parente *et al.*, 2007; Burla *et al.*, 2008; Vahrenkamp, 2010; Huck *et al.*, 2011; Schmitt *et al.*, 2020). Syn-depositional and post-depositional diagenetic alteration (Allan & Matthews, 1982; Oehlert & Swart, 2014, 2019) as well as biological fractionation and local palaeoceanographic

conditions may cause the $\delta^{13}\text{C}$ composition of shallow-water carbonates to deviate from the global open ocean value (Patterson & Walter, 1994; Immenhauser *et al.*, 2008; Huck *et al.*, 2017). A positive covariance between $\delta^{13}\text{C}$ and $\delta^{18}\text{O}$ bulk values is often used to infer either decreasing alteration in the freshwater phreatic zone (Swart & Oehlert, 2018) or diagenetic alteration under the meteoric water influx in the mixing zone (Allan & Matthews, 1982). As a result, several studies proposed the lack of covariance between $\delta^{13}\text{C}$ and $\delta^{18}\text{O}$ values as indicative of the unaltered nature of samples (e.g. Grotzinger *et al.*, 2011). Nevertheless, recent studies point out that a lack of correlation between $\delta^{13}\text{C}$ and $\delta^{18}\text{O}$ alone cannot be used as proof for sample preservation, and that changes in sediment source through time can also produce paired shifts in $\delta^{13}\text{C}$ and $\delta^{18}\text{O}$ values (Swart & Oehlert, 2018; Oehlert & Swart, 2019).

In the studied sections, scatterplots of $\delta^{13}\text{C}$ and $\delta^{18}\text{O}$ show no significant correlation for individual lithofacies or for lithofacies associations (Fig. 9A and B), suggesting that variations in $\delta^{13}\text{C}$ are not the result of facies changes. In the analysed samples, most of the isotope bulk values are coherent with the rudist and *Chondrodonta* shells isotope values.

The analysed samples partly overlap the Aptian isotopic field of the Apennine Platform shallow-water carbonates (Di Lucia *et al.*, 2012; Schmitt *et al.*, 2020) and plot within the lower range of Barremian – Aptian seawater (‘low-latitude’) biotic calcite field of Prokoph *et al.* (2008) (Fig. 9C). With respect to the field of the Aptian Apennine Platform shallow-water carbonates, an important tail of more depleted $\delta^{13}\text{C}$ and $\delta^{18}\text{O}$ values is observed. The moderate inverted ‘J’ stable isotope pattern (more visible

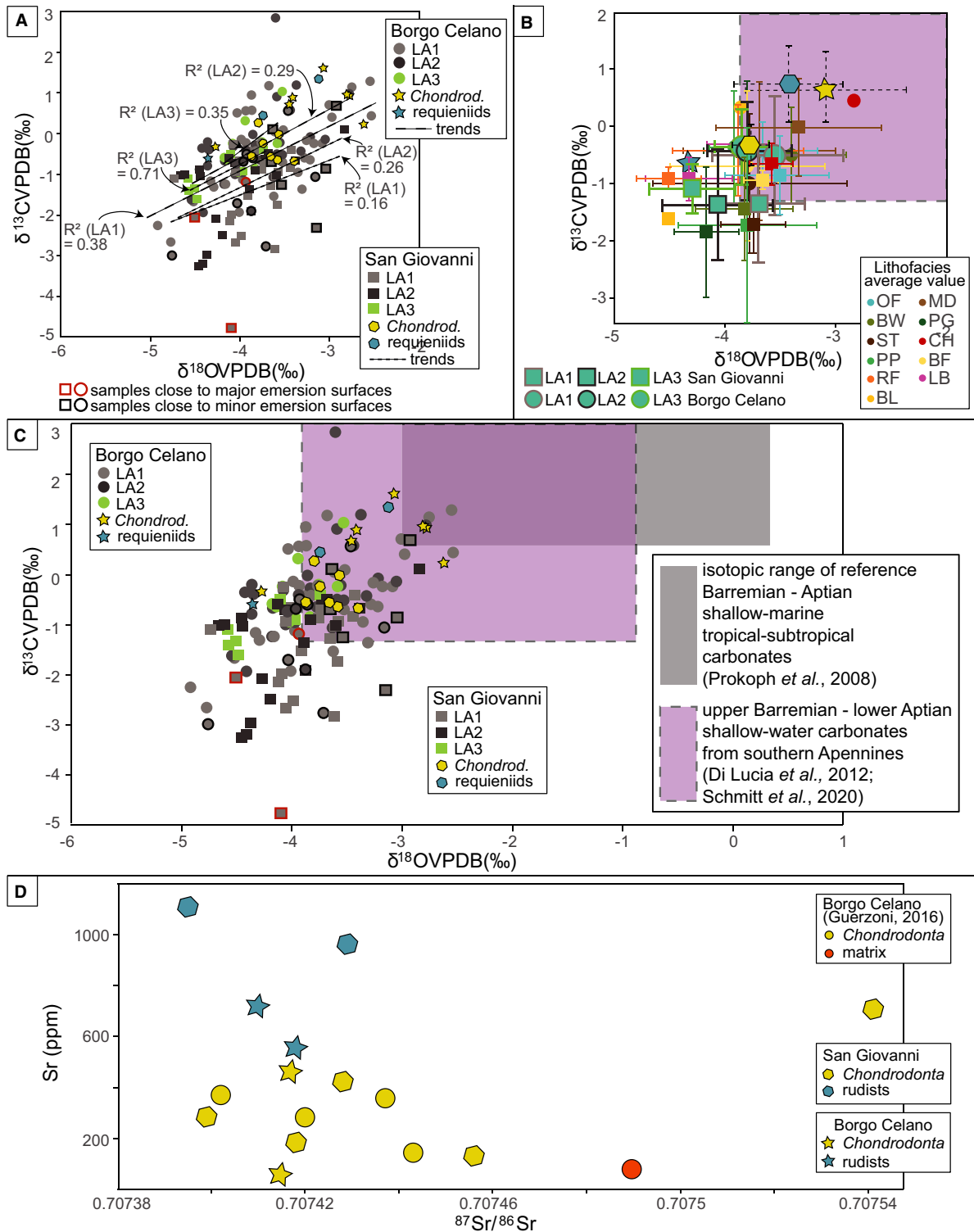


Fig. 9. Scatterplots of the C and O isotopic values of the San Giovanni and Borgo Celano sections. (A) C and O correlation for the bulk of each lithofacies association and for *Chondrodonta* and requieniid shells. (B) C and O average correlation for single lithofacies and lithofacies associations. (C) Scatterplots of the studied sections against the isotopic range of both the Barremian – Aptian shallow-marine tropical–subtropical carbonates by Prokoph et al. (2008) and the Barremian – lower Aptian shallow-water carbonates of the Apennine Platform (Di Lucia et al., 2012; Schmitt et al., 2020). (D) Correlation between the concentration of Sr (ppm) and the $^{87}\text{Sr}/^{86}\text{Sr}$ value in *Chondrodonta* and requieniid shells, compared to Borgo Celano shell samples analysed by Guerzoni (2016).

for the San Giovanni section; see Fig. 9A and C) indicates an impact of meteoric diagenesis (Allan & Matthews, 1982; Lohmann, 1988), mainly affecting LA1 and LA2 facies. In the presented dataset, LA1 and, subordinately, LA2 facies, contain frequent exposure-related features like spar-filled fenestrae, micro-vugs and thin intraformational brecciated levels (Fig. 9A and C). Despite this evidence of meteoric alteration, not all samples located below emersion surfaces have negative $\delta^{13}\text{C}$ values and also not all samples with negative $\delta^{13}\text{C}$ values are associated with exposure surfaces. These findings confirm the complexity of the stable isotopes' behaviour in shallow-water carbonates associated with exposures (e.g. Immenhauser *et al.*, 2003; Theiling *et al.*, 2007; Christ *et al.*, 2012) and suggest that some negative excursions may be related to changes in the primary marine carbon isotope signal.

Considering the potential for diagenetic effects, a conservative approach was chosen for the use of $\delta^{13}\text{C}$ profiles for stratigraphic correlations (e.g. Huck *et al.*, 2017). All samples with evidence of exposure/dissolution features at the outcrop or microscope scale were discarded and a smoothing procedure was run to highlight low-order trends and excursions in $\delta^{13}\text{C}$. The general trend of $\delta^{13}\text{C}$ values is more likely to record the long-term global variations of the open ocean than higher-order fluctuations; the latter are more likely to result from variations in local environmental conditions on the shallow platform (Colombie *et al.*, 2011).

The overall isotope trends and excursions, which extend across multi-metre-thick intervals at both San Giovanni and Borgo Celano, can be traced and correlated across the two sections (for example, the positive $\delta^{13}\text{C}$ peak at the top of the *Chondrodonta* bedsets, which precedes a decreasing trend of the curve). This evidence suggests that isotopic patterns in the smoothed data are, therefore, significant and reflect a control overriding the local-scale diagenetic processes.

The outer low-Mg calcite layer of Cretaceous rudist and oyster shells has been widely recognized as a suitable archive for the Sr-isotope composition of ocean waters (e.g. Steuber *et al.*, 2005; Boix *et al.*, 2011; Frijia *et al.*, 2015; Huck & Heimhofer, 2015). The concentration of strontium, iron and manganese in shells is commonly used for estimating the degree of diagenetic alteration (e.g. Ullmann & Korte, 2015) and

several elemental threshold values have been suggested for both rudists (Fe < 100 ppm, Mn < 50 ppm, Sr > 700 ppm; Steuber *et al.*, 2005; Frijia *et al.*, 2015) and *Chondrodonta* (Mn < 250 ppm, Sr > 500 ppm; Damas Mollá *et al.*, 2006). Considering that diagenesis is usually associated with a decreased Sr concentration coupled with increased Fe – Mn concentrations and increased $^{87}\text{Sr}/^{86}\text{Sr}$ ratios, only shells with low iron and manganese concentrations in skeletal calcite and high strontium concentrations are, usually, considered suitable for Strontium Isotope Stratigraphy (SIS).

In the presented dataset, all shell samples have Fe and Mn concentrations below the conventional thresholds indicative of diagenetic resetting and they show no covariance with Sr concentrations (Table 2). The Sr content is higher in rudist shells (558 to 1109 ppm) than in *Chondrodonta* shells (57 to 708 ppm), as also observed by Schmitt *et al.* (2020) in samples from the Apennine Platform. No correlation between decreasing Sr content and increasing/decreasing $^{87}\text{Sr}/^{86}\text{Sr}$ in rudists and *Chondrodonta* shells (Fig. 9D) as well as no covariance of Sr concentration with $\delta^{13}\text{C}$ or $\delta^{18}\text{O}$ values, were observed. Only one sample from the *Chondrodonta* bedset of San Giovanni, despite its high Sr concentration, yields an $^{87}\text{Sr}/^{86}\text{Sr}$ value higher than the isotope composition of the sample matrix (sample DPG11-A; see Table 2). On the other hand, a few samples with low Sr concentration also have low $^{87}\text{Sr}/^{86}\text{Sr}$ values (Table 2). This evidence indicates that strict thresholds in Fe, Mn and Sr concentrations are not perfect screening mechanisms for identifying samples with primary isotope ratios.

Internal consistency of Sr isotopic values among different components within the same bed or nearby beds is, instead, considered as strong evidence for preservation of the original signal (McArthur *et al.*, 2004, 2012). Therefore, samples with elemental concentrations below the published elemental threshold values (for example, Sr > 500 ppm for *Chondrodonta* and Sr > 700 ppm for rudists) were considered for SIS only when their Sr-isotope values were within the analytical error (8×10^{-6} in average) with respect to other shells from the same bed or from the nearby beds. Only one sample (SG14-D; see Table 2), despite its internal consistency of the Sr isotopic value, was discarded for the SIS due to a lower Sr concentration with respect to the one measured in the matrix.

Table 2. Elemental concentrations and Sr-isotope ratios of the studied ruditid and *Chondrodonta* samples collected from the San Giovanni and the Borgo Celano 1 sections. Sr-isotopes values have been corrected for interlaboratory bias (see text for further details). Preferred numerical ages have been derived from the look-up table of McArthur et al. (2001, version 5: 04/2013), which is calibrated to the Geological Time Scale of Ogg & Finnov (2012). See the text for details on the precision estimation and on the calculation of minimum and maximum ages. In italics, samples discharged from the Strontium Isotope Stratigraphy (SIS); in bold, the mean value of the Sr isotope ratio for each sample set and the preferred numerical age derived from it. Minimum and maximum ages were obtained by combining the statistical uncertainty (2 SE) of the mean values of the Sr-isotope ratios with the uncertainty of the seawater curve (see Frijia et al., 2015, for details on the procedure).

Location	Sample	Component	$^{87}\text{Sr}/^{86}\text{Sr}$ measured	± 2 SE (* 10^{-6})	$^{87}\text{Sr}/^{86}\text{Sr}$ corrected	± 2 SE mean (* 10^{-6})	Mg ($\mu\text{g/g}$)	Sr ($\mu\text{g/g}$)	Fe ($\mu\text{g/g}$)	Mn ($\mu\text{g/g}$)	Min.	Age (Ma) preferred	Max.
San Giovanni	DPG11-A	<i>Chondrodonta</i>	0.707538	19	0.707541	1847	708	91.9	4.93				
	DPG10B-E	<i>Chondrodonta</i>	0.707453	9	0.707456	1266	130	46.5	4.36				
	DPG10B-C	<i>Chondrodonta</i>	0.707425	5	0.707428	1670	423	100.0	2.77				
	DPG10B-F	<i>Chondrodonta</i>	0.707415	6	0.707418	1362	181	38.5	2.87				
	DPG11D-B	<i>Chondrodonta</i>	0.707396	7	0.707399	1705	283	40.0	1.76		125.2	125.87	126.35
	DPG11-m	Matrix		Mean	0.707415	21	1351	66	179.0	5.0			
Borgo Celano	DPG38-A	Requeniid	0.707415	5	0.707395	1075	1109	35.0	0.9				
	DPG37-A	Requeniid	0.707426	18	0.707429	1021	963	29.8	1.2		124.55	125.75	126.65
	DPG37-m	Matrix		Mean	0.707412	34	1156	61	128.0	4.0			
	BCG3-1	Requeniid	0.707404	5	0.707410	1718	720	37.0	3.46				
Borgo Celano	SG14-D	<i>Chondrodonta</i>	0.707412	6	0.707415	1713	57	42.0	11.5		124.48	125.65	126.60
	BCG-m	Matrix		Mean	0.707410	34	1949	96	185.0	10.0			
	SG6B-A	Requeniid	0.707415	4	0.707418	979	558	7.42	5.63				
	SG6B-B	Requeniid	0.707419	6	0.707422	na	na	na	na				
	SG6A	<i>Chondrodonta</i>	0.707414	5	0.707417	2589	463	34.8	3.54		125.9	125.98	126.08
	SG6-m	Matrix		Mean	0.707419	3	1543	73	136.0	9.0			

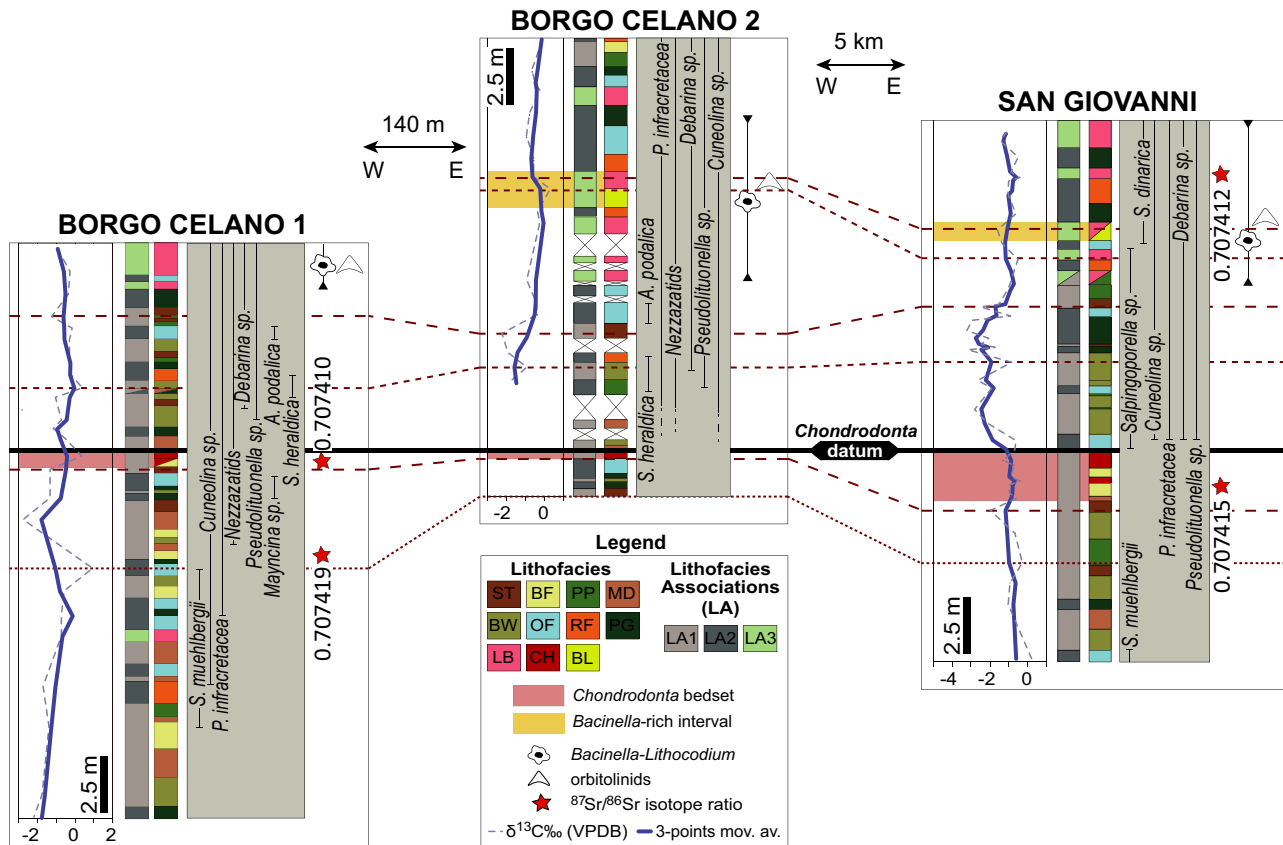


Fig. 10. Attempt at correlation between the investigated sections based on SIS, biostratigraphy, $\delta^{13}\text{C}$ curves and the vertical evolution of lithofacies. The top of the *Chondrodonta* bedsets is here used as datum. See *Lithofacies and lithofacies associations* section and Table 1 for the description of lithofacies and lithofacies associations.

Correlation of the stratigraphic sections

The integrated high-resolution framework based on biostratigraphy, SIS and $\delta^{13}\text{C}$ segments enables correlation of lithofacies and lithofacies associations. The benthic foraminiferal assemblage at the base of the three sections (Figs 4, 6A and 7A), including *Cuneolina* sp., *P. infracretacea*, *Mayncina* sp. and the last occurrence of the dasycladacean alga *S. muehlbergii* (0.5 m at San Giovanni and 11 m at Borgo Celano), indicates a lowermost Aptian age (Chiocchini *et al.*, 2012). Above the *Chondrodonta* bedsets, the co-occurrence of *Debarina* sp., *Pseudolituonella* sp. and *S. dinarica* indicates either an early (Chiocchini *et al.*, 2012) or early – late (Di Lucia *et al.*, 2012) Aptian age. The co-occurrence of *M. lotzei* and *P. cormyi* within the uppermost part of the Borgo Celano 2 section (see also Claps *et al.*, 1996) suggests a late early Aptian or, possibly, an early late Aptian age, according to the most recent review of Schröder *et al.* (2010).

The mean $^{87}\text{Sr}/^{86}\text{Sr}$ from the *Chondrodonta* bedset at San Giovanni (0.707415) and at Borgo Celano (0.707410) are statistically indistinguishable (see Table 2), suggesting that the two *Chondrodonta* bedsets are roughly coeval. The first occurrence of *Debarina* sp. a few metres above the top of the *Chondrodonta* bedsets, supports this interpretation. The isotopic values indicate an estimated age of 125.87 ± 0.6 Ma at San Giovanni and of 125.65 ± 1 Ma at Borgo Celano, corresponding to the lower part of the early Aptian, consistent with the biostratigraphic data. Samples of a bivalve floatstone 5 m below the *Chondrodonta* bedset at Borgo Celano have an $^{87}\text{Sr}/^{86}\text{Sr}$ mean value of 0.707419, calibrated to an age of $125.98 \text{ Ma} \pm 0.1$. A rudist floatstone 12 m above the *Chondrodonta* bedset at San Giovanni has a value of 0.707412, calibrated to an age of $125.75 \text{ Ma} \pm 1$. The similar $^{87}\text{Sr}/^{86}\text{Sr}$ values among sections constrain the age of the *Chondrodonta* bedsets within the early Aptian at the boundary between *Globigerinelloides*

biotic changes reflect a stressed platform ecosystem during the deposition of the lower Aptian San Giovanni Rotondo Limestone, preventing the thriving of a diversified macro-benthic and micro-benthic fauna. Similar biotic turnovers, indicative of environmental stress, have been documented worldwide during the early Aptian (Huck *et al.*, 2010; Rameil *et al.*, 2010; Skelton & Gili, 2012; Stein *et al.*, 2012; Huck *et al.*, 2014; Núñez-Useche *et al.*, 2020, among others).

Relative sea-level fluctuations in the stratigraphic sections are indicated by both ephemeral emersion-related features in the lower part and by a facies shift towards open shelf deposits in the middle-upper part. These fluctuations can be attributed either to decreased carbonate production or to eustatic changes.

Along the margin of the Apulia Carbonate Platform (ACP), a pronounced lower Aptian backstepping of at least 5 km landward is indicated by pelagic facies (Marne a Fucoidi formation) overlying the slope and margin succession. This backstepping, interpreted as a drowning unconformity (Bosellini *et al.*, 1999a; Graziano, 2013) or as a partial drowning (Morsilli *et al.*, 2017), is coeval with the drowning phase documented in many other lower Aptian Tethyan platforms (Bover-Arnal *et al.*, 2012; Husinec *et al.*, 2012; Maurer *et al.*, 2013; Pictet *et al.*, 2015, among others). However, no high-resolution sequence stratigraphic studies of the lower Aptian inner platform facies on the ACP have been carried out to date and the short stratigraphic interval analysed in this study prevents a broader scale comparison to track sea-level changes at a regional or global scale.

Platform-to-basin correlation

The $\delta^{13}\text{C}$ record of the studied sections can be used in combination with biostratigraphic markers and SIS to achieve a chemostratigraphic correlation with the $\delta^{13}\text{C}$ curves of the Cismon Apticore in southern Alps (Menegatti *et al.*, 1998; Erba *et al.*, 1999) and of the Adriatic Basin adjacent to the ACP (Luciani *et al.*, 2001, 2006) (Fig. 11).

The beginning of the negative $\delta^{13}\text{C}$ trend in the studied sections (1.6 m at San Giovanni and 11.1 m at Borgo Celano) is correlative with the top of the magnetochron M0 of Malinverno *et al.* (2010), right below the onset of the C3 segment in the Cismon section. The chemostratigraphic Selli Event (C3–C6 segments, *cf.* Erba *et al.*, 1999; Malinverno *et al.*, 2010) is here placed

within the middle-upper part of the San Giovanni section and in the lower part of Borgo Celano composite. The beginning of the C3–C4 segments within the Cismon Apticore is correlated with the negative shift right above the *Chondrodonta* bedsets (Fig. 11). The positive shift of the C6 segment in the Cismon Apticore is tentatively correlated with the *Bacinella*-rich level. Higher in the Borgo Celano composite section, the increasing $\delta^{13}\text{C}$ values associated with thick stromatolite beds are tentatively correlated to the C7 segment. According to this interpretation, the San Giovanni and the Borgo Celano $\delta^{13}\text{C}$ curves would capture the entire perturbations of the global carbon cycle associated with OAE1a, including their prelude in the upper C2 segment.

This chemostratigraphic correlation places the *Chondrodonta* bedsets within the uppermost C2 segment, making them coeval with the *Chondrodonta* accumulations of the Monte degli Angeli Limestone margin facies (see Graziano, 2013; Guerzoni, 2016) exposed along the southern Gargano Promontory (Fig. 1A).

The San Giovanni section and the lower part of the Borgo Celano composite have been further correlated to the $\delta^{13}\text{C}$ curve of the Coppitella section in the Adriatic Basin. This section represents the pelagic deposits of the ‘Marne a Fucoidi’ (Fig. 1A). Black shales occur at Coppitella only in the C6–C7 segments (*cf.* ‘lower’ and ‘upper’ black shales in Luciani *et al.*, 2001, 2006), are absent in the C3–C4 segments and not exposed in the C5 segment (see Fig. 11).

The quantitative micropalaeontological analysis carried out by Luciani *et al.* (2001) on planktonic and small benthic foraminifera, calcareous nannofossils and radiolarians indicates oligomesotrophic conditions in the C3–C5 tract, suggesting that Coppitella did not record the eutrophication affecting the global oceans during most of OAE1a (Menegatti *et al.*, 1998; Jenkyns, 2003; Erba & Tremolada, 2004). Moderate and high fertility conditions have been interpreted for the ‘lower’ (C6 segment) and ‘upper’ (middle C7 segment) black shales, respectively (see figs 6 to 9 in Luciani *et al.*, 2001).

Both the micropalaeontological associations and the stratigraphic position of black shales in basinal settings suggest that eutrophication occurred only from the upper part of OAE1a interval in the Adriatic Basin (i.e. from the C6 segment). The same time interval was characterized by biotic turnovers in the shallow-water settings of the ACP. Indeed, the gradual

disappearance of rudists in favour of orbitolinids and *Bacinnella–Lithocodium* assemblages would indicate a gradual shift from oligotrophic to mesotrophic conditions across OAE1a, according to the nutrient gradients for benthic communities proposed by Mutti & Hallock (2003) and Rameil *et al.* (2010).

The chemostratigraphic C3–C4 segments (Fig. 11) correlate in the studied sections with an interval of peloidal packstone–grainstones and lime mud-rich facies with scarce to absent skeletal components like molluscs, foraminifera and dasycladales (see Figs 4, 6A and 7A). This decreased abundance of organisms indicates deposition under stressed conditions during the first part of OAE1a, as also suggested by the trace element concentrations in the San Giovanni section (Fig. 5). A suite of RSTE (V, As, Mo and U) has been used to better reconstruct the palaeoredox conditions (see Tribovillard *et al.*, 2006; Hueter *et al.*, 2019) and the P/Al ratio has been used to track the nutrient content of the seawater (e.g. Föllmi, 1995; Westermann *et al.*, 2013). The changes in concentration of RSTE should be observed at different temporal scales due to their variable residence time in the oceans (from few kyr to hundreds of kyr; Sholkovitz & Schneider, 1991; Shields & Stille, 2001; Bodin *et al.*, 2007). Nevertheless, due to the different solubility of V, Mo and U in waters with variable levels of oxygen, decreases in the RSTE concentration in marine deposits are commonly assigned to an oxygen deficiency phase favouring the enrichment of RSTE in organic-rich sediments (Algeo & Maynard, 2004; Tribovillard *et al.*, 2006; Bodin *et al.*, 2007; Hueter *et al.*, 2019). The decrease of the RSTE/Al ratios in the San Giovanni section within the chemostratigraphic C3–C4 segments suggests dysaerobic conditions during the first part of OAE1a, thus reinforcing the sedimentological data. A similar decrease in RSTE from the base of the C3 segment has been observed in the Adriatic Platform (Hueter *et al.*, 2019). The decreased RSTE correlate with a decrease of the P/Al ratio (Fig. 5), indicative lower nutrient content. Dysaerobic seawater and lower nutrient levels may explain, therefore, the impoverished fauna in the C3–C4 segments.

Stressed conditions on the ACP in the lower part of OAE1a are further suggested by the gamma ray profiles of the Borgo Celano 1 section (see Fig. 6B). The increase in the total API (%) and, particularly, in uranium (ppm) across the C3–C4 tract may indicate a progressive enrichment in organic matter. Similar trends, with a

marked gamma ray peak caused by an increased concentration of uranium, have been observed in the lower part of the Shu'aiba Formation in northern Oman (Vahrenkamp, 2010). The OAE1a interval in the Shu'aiba Formation (*cf.* 'Maximum Flooding Interval'; see Vahrenkamp, 2010) is marked by a gamma ray peak caused by the uranium, interpreted as indicative of an enrichment in organic matter.

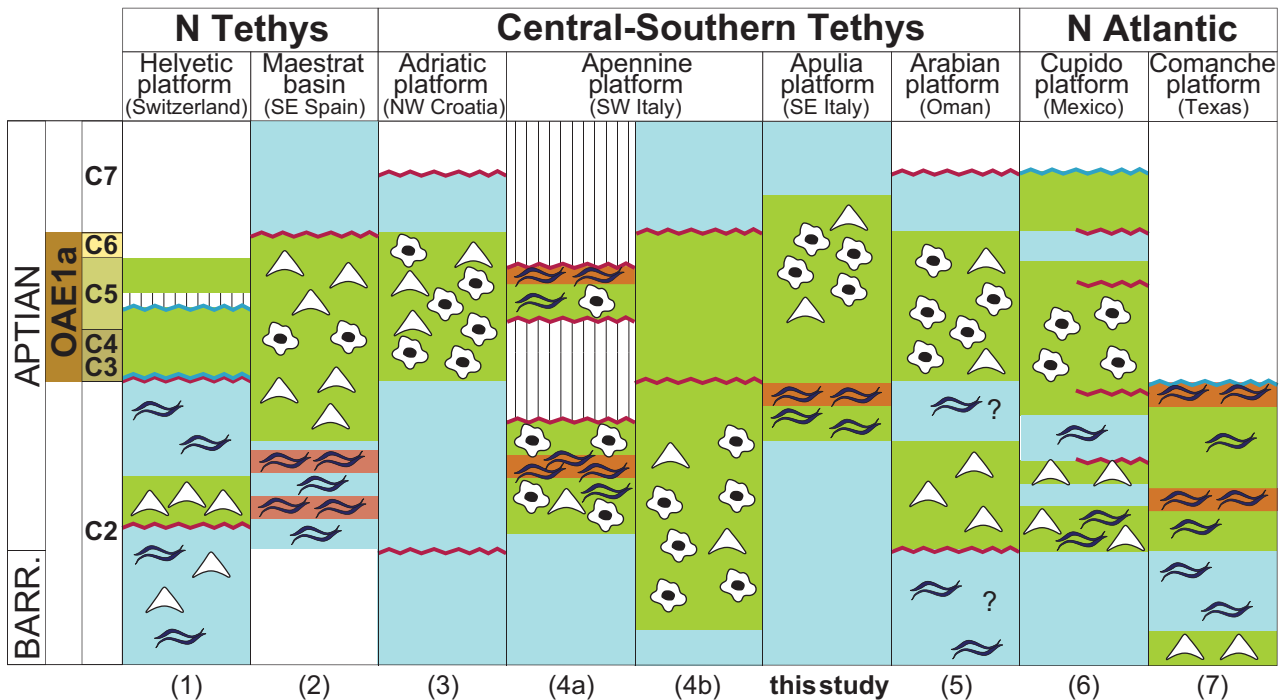
The enrichment in organic matter at Borgo Celano also correlates with a global biocalcification crisis (Weissert & Erba, 2004; Erba *et al.*, 2010; Giraud *et al.*, 2018), carbonate platform drowning in northern Tethys, and biotic turnover (from rudist-dominated to *Bacinnella–Lithocodium*-dominated) on carbonate platforms of the Southern Tethys (e.g. Skelton & Gili, 2012; Huck *et al.*, 2014).

Upward in the studied sections, the *Bacinnella*-rich level correlates to the chemostratigraphic C6 segment, characterized by mesotrophic conditions (i.e. moderate fertility peak, see above) and the deposition of the 'lower' black shale in the Adriatic Basin (Fig. 11). Increased nutrient input on the ACP in this tract is also suggested by the more open-shelf facies of the coeval Coppa di Pila limestones (northern Gargano; Fig. 1A). Here, orbitolinid-rich mudstones with subordinate *Bacinnella–Lithocodium* micro-encrustations are overlain by foraminifera-rich and bivalve-rich beds, indicative of restoration of normal-marine conditions (Guerzoni, 2016).

Transient peaks in the abundance of *Bacinnella–Lithocodium*, coeval with black shale deposition during OAE1a, also occur on the Arabian and Adriatic platforms (Huck *et al.*, 2010; Rameil *et al.*, 2010) and have been interpreted to reflect meso-eutrophic conditions on the platform top.

The smaller magnitude bloom of *Bacinnella–Lithocodium* on the ACP, with respect to the Arabian and Adriatic platforms, can be attributed to moderate nutrient levels on the platform top, coeval to the only moderate fertility conditions in the Adriatic Basin.

A transgressive and deepening-up trend is further interpreted at the base of the *Bacinnella–Lithocodium* interval on the Arabian and Adriatic platforms (Huck *et al.*, 2010). On the ACP, a transgressive episode at the base of the *Bacinnella–Lithocodium* facies is suggested by the deepening-up trend interpreted from open shelf LA2 deposits progressively replacing restricted subtidal LA1 facies in the C5–C6 segments (see Figs 4, 6A and 10).



Legend


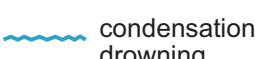


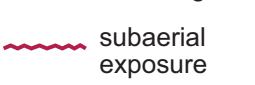


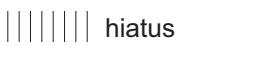

	limestones with oligotrophic associations		condensation/drowning		orbitolinids
	limestones with meso- to eutrophic associations		subaerial exposure		<i>Bacinella-Lithocodium</i>
	<i>Chondrodonta</i> bedset; monospecific or quasi-; individuals in up-right position		hiatus		inferred occurrence of <i>Chondrodonta</i>

Fig. 12. Synthesis of the occurrence of *Chondrodonta* within worldwide inner platform carbonates during the main biotic, environmental and stratigraphic events spanning the uppermost Barremian – lower Aptian (including OAE1a) interval. The stratigraphic sections (not to scale) have been reported and integrated from: (1) Wissler *et al.* (2003) and Föllmi *et al.* (2006), (2) Malchus *et al.* (1995) and Bonin *et al.* (2016), (3) Huck *et al.* (2010), (4a) Graziano & Raspini, 2018, (4b) Amodio & Weissert (2017), (5) Pittet *et al.* (2002), Immenhauser *et al.* (2004), Rameil *et al.* (2010) and Huck *et al.* (2010), (6) Núñez-Useche *et al.* (2020), (7) Phelps *et al.* (2014, 2015). Graphics inspired by Amodio & Weissert (2017).

Proliferation of *Chondrodonta*: proxy of ecological stress in shallow-water communities prior to OAE1a?

Regional occurrence of *Chondrodonta* accumulations

Few studies on Berriasian – lower Barremian shallow-water carbonates report *Chondrodonta* accumulations in the Southern Tethys (e.g. Pratt & Smewing, 1990; Zaghbib-Turki, 2003; Masse *et al.*, 2015) and in the proto-North Atlantic (e.g. Phelps *et al.*, 2014). In contrast, upper Barremian – lower Aptian *Chondrodonta* accumulations have been extensively documented

worldwide. With few exceptions (Posenato *et al.*, 2018, 2020), only limited attention has been given to the palaeoecological significance of *Chondrodonta* accumulations. Only a few authors (e.g. Phelps *et al.*, 2015; Posenato *et al.*, 2018; Núñez-Useche *et al.*, 2020) have interpreted *Chondrodonta* as an indicator of ecological stress in a mesotrophic domain. Other authors (e.g. Leonide *et al.*, 2012; Bonin *et al.*, 2016) consider it as a component of oligotrophic (cf. ‘Urgonian’) communities.

Determining the precise stratigraphic position of every *Chondrodonta* bed reported worldwide

is challenging. Only by integrating recent high-resolution studies on the stratigraphic, environmental and ecological evolution of worldwide carbonate platform successions spanning OAE1a, a synthesis of the global accumulations was feasible (Fig. 12).

In the Helvetic domain (Switzerland) of the Northern Tethys, *Chondrodonta* occurs within oligotrophic coral–rudist limestones (Wissler *et al.*, 2003) of the uppermost Barremian – lower Aptian succession, below the drowning interval associated with mesotrophic associations (Föllmi *et al.*, 2006). *Chondrodonta* also occurs both in rudist limestones and in monospecific biostromes in the (?) upper Barremian – lower Aptian carbonates of Hungary (Császár *et al.*, 1994), below an interval with abundant *Bacinnella–Lithocodium* and orbitolinids. In the Maestrat Basin (south-east Spain), *Chondrodonta* occurs in monospecific biostromes prior to OAE1a (Malchus *et al.*, 1995) but is interpreted as recording ‘normal marine conditions’ (Bonin *et al.*, 2016). In the Vocontian Basin and Provence Platform domains (south-east France), stepwise drowning events prior to OAE1a (Masse & Fenerci-Masse, 2013; Giraud *et al.*, 2018) are characterized by Urgonian limestones with episodic orbitolinid levels. Leonide *et al.* (2012) report local chondrodontids in Urgonian rudist facies, extending to the uppermost chemostratigraphic C2 segment.

In the Central and Southern Tethyan realm, the upper Barremian – lower Aptian Apennine Platform (Amodio & Weissert, 2017) is characterized by a shift towards mesotrophic conditions with *Bacinnella–Lithocodium* and *Palorbitolina lenticularis*. Graziano & Raspini (2018) interpret abundant *Chondrodonta*, both in monospecific biostromes and in association with *Bacinnella–Lithocodium* and *P. lenticularis*, as an indication of mesotrophic conditions. Orbitolinid-rich rocks of earliest Aptian age and extensive *Bacinnella–Lithocodium* intervals at the turn of OAE1a occur in Oman (Pittet *et al.*, 2002; Huck *et al.*, 2010; Rameil *et al.*, 2010); here *Chondrodonta* floatstones are interpreted as oligotrophic communities proliferating probably up to the uppermost C2 segment, although ‘abundant oysters’ (*cf.* Immenhauser *et al.*, 2004) are also reported within *Bacinnella–Lithocodium* facies. Rudist–*Chondrodonta* limestones interbedded with orbitolinid-rich beds occur in the (?) lower Aptian shallow-water successions of Ethiopia (Bosellini *et al.*, 1999b) and Somalia

(Barbieri *et al.*, 1979) and in the (?) Barremian – Aptian limestones of Afghanistan (Abdullah *et al.*, 2008).

In the proto-North Atlantic, Najarro *et al.* (2011) report *Chondrodonta* within oligotrophic assemblages of the Basque–Cantabrian Basin that underlie and overlie OAE1a. Conversely, in the Lusitanian Basin (Portugal), Huck *et al.* (2014) interpret the replacement of oligotrophic rudist–coral limestones by orbitolinid–oyster-rich facies with subordinate *Bacinnella–Lithocodium*, as a result of palaeoenvironmental perturbations and incipient drowning associated with OAE1a. In the Gulf of Mexico, *Chondrodonta* occurs in association with *Bacinnella–Lithocodium* in (?) Barremian – lower Aptian limestones of the Atima Platform in Honduras (Scott & Finch, 1999). In the Comanche Platform (Texas) Phelps *et al.* (2014, 2015) report *Chondrodonta* within upper Barremian rudist limestones and as lower Aptian monospecific biostromes (up to the top of the C2 segment) and interpret them as a response to increased detrital clay input, preceding sea-level transgression and platform drowning during OAE1a. Similarly, in the Cupido Platform (Mexico) which drowned after OAE1a, Núñez-Useche *et al.* (2020) interpret the occurrence of lowermost Aptian orbitolinid-rich and *Chondrodonta*-rich beds as a short mesotrophic event caused by both sea-level transgression and increased continental weathering due to a more humid climate. *Chondrodonta* in the Cupido Platform occurs also within oligotrophic assemblages at the onset of OAE1a, below an extensive *Bacinnella–Lithocodium* interval recording environmental instability and mesotrophic conditions during the anoxic event.

Globally (Fig. 12), *Chondrodonta* thrived both within coral–rudist associations (as a subordinate component) as well as in fully mesotrophic conditions (where it predominates) and, except for the Apennine Platform, its accumulations generally pre-date the strong environmental stress that affected shallow-water carbonates deposition during OAE1a.

Palaeoenvironmental controls on the Chondrodonta proliferation

During OAE1a, environmental disturbances triggered by the Barremian–Aptian climate warming (Larson, 1991; Larson & Erba, 1999; Tejada *et al.*, 2009) caused biotic stress in the shallow-water and deep-water domains (e.g. Pancost

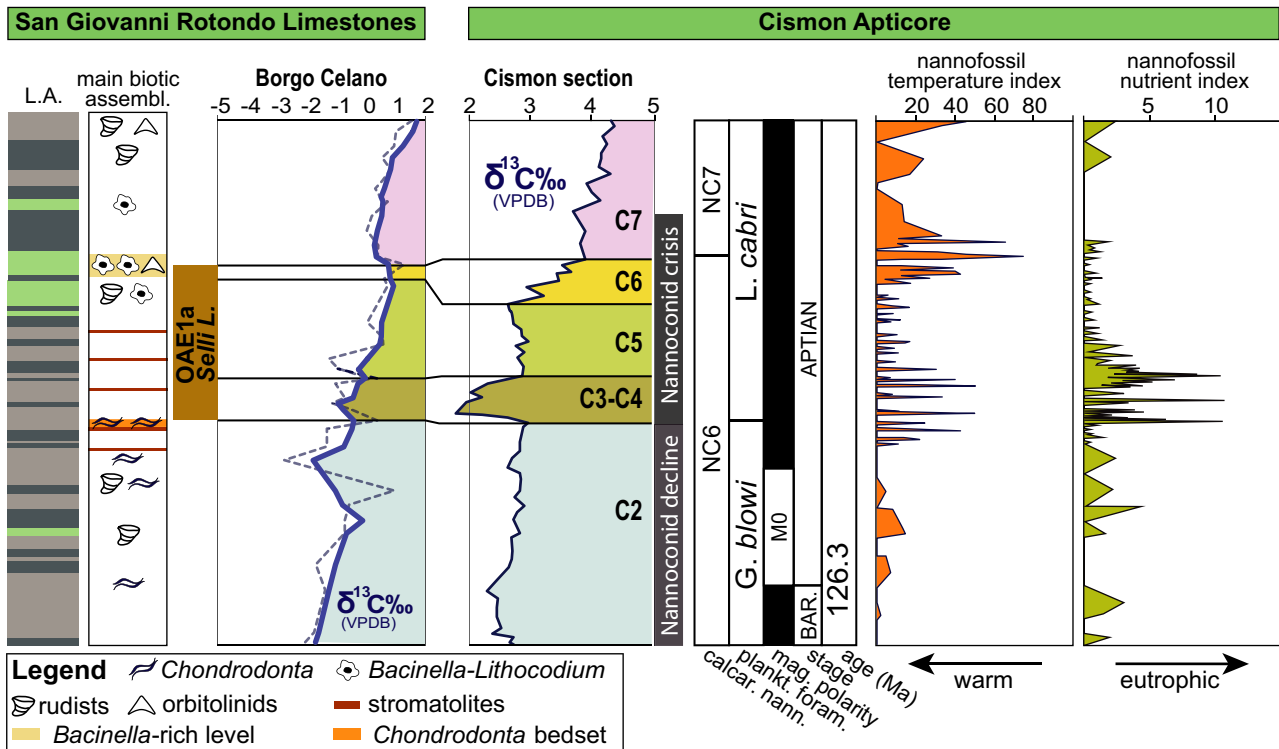


Fig. 13. Attempt to reconstruct the palaeoenvironmental fluctuations influencing the proliferation of *Chondrodonta* within the lower Aptian San Giovanni Rotondo Limestone (SGRL). The main biotic events in the studied sections are compared to the temperature and nutrient fluctuations in the nearby pelagic realm of the Cison section. The $\delta^{13}\text{C}$ curve of the Cison Apticore has been taken from Erba *et al.* (1999), the nannofossil and planktonic foraminiferal biostratigraphy is from Weissert & Erba (2004); the nomenclature of the C-isotope C2 – C7 segments is from Menegatti *et al.* (1998) and the Nannoconid decline and crisis intervals as well as the magnetic polarity are from Malinverno *et al.* (2010); the nannofossil temperature and nutrient indexes are from Bottini *et al.* (2015); the numerical age of the Barremian – Aptian boundary is after Ogg & Hinnov (2012). See Fig. 4 and Table 1 for the description of lithofacies associations.

et al., 2004; Dumitrescu *et al.*, 2006; Föllmi *et al.*, 2006; Najarro *et al.*, 2010). Ocean eutrophication (i.e. ‘nannoconid crisis’; Erba, 1994, 2004) and carbonate platform demise (Weissert *et al.*, 1998; Wissler *et al.*, 2003) are widely documented. Intensified precipitation and continental weathering due to a warmer and more humid climate, combined with increased upwelling near coastlines due to intensified atmospheric and oceanic circulation, increased the nutrient (for example, phosphorous) input to shallow-water areas (Föllmi, 1996, 2012). The latter resulted in biotic turnover from oligotrophic to mesotrophic benthic communities on the platform top during OAE1a (e.g. Immenhauser *et al.*, 2005; Skelton & Gili, 2012; Huck *et al.*, 2014; Amodio & Weissert, 2017; Hueter *et al.*, 2019). Nevertheless, biotic changes in the shallow-water benthic communities occurred also in the prelude phase of the anoxic event.

Chondrodonta is considered an opportunistic and r-strategist taxon and a relatively high nutrient availability has been suggested as a prerequisite for its thriving (Posenato *et al.*, 2018, 2020). This interpretation is supported by the stratigraphic occurrence of the studied *Chondrodonta* bedsets on the ACP, in an interval of transition from oligo-mesotrophic (i.e. rudists) to fully mesotrophic (i.e. *Bacinella-Lithocodium*, orbitolinids) biotic assemblages. A relative increase in the P/Al concentration and its trend within the *Chondrodonta* bedset of the San Giovanni section (see Fig. 5) suggest higher and fluctuating trophic levels during its deposition. These nutrient fluctuations, which occur just below the onset of OAE1a, correlate with the oligo-mesotrophic regime in the Adriatic Basin (see *Platform-to-basin correlation* section) and with increasing eutrophication in the nearby pelagic Cison Apticore (Fig. 13; see Bottini

et al., 2015). The latter correlation suggests a local to regional scale increase of trophic sources, as also confirmed by the stratigraphic position of the worldwide lower Aptian *Chondrodonta* beds, placed in a transitional phase between oligotrophic and mesotrophic communities (Fig. 12). Stratigraphic evidence on the major sources of P on the ACP during the deposition of the *Chondrodonta* bedsets, however, still needs to be investigated.

Most worldwide *Chondrodonta* accumulations can be correlated to a short interval preceding the onset of OAE1a (Fig. 12); in some cases, the accumulations extend also within the anoxic event and even slightly above (for example, Apennine Platform; Graziano & Raspini, 2018), whereas in other areas they have not been reported (for example, Adriatic Platform; Huck *et al.*, 2010). These observations suggest that the proliferation of *Chondrodonta*, mainly triggered by increased nutrient availability, would have been favoured or prevented by other local and/or regional environmental fluctuations during the early Aptian.

The facies analysis of the *Chondrodonta* bedsets on the lower Aptian ACP indicates a low-energy and restricted subtidal environment during their deposition. The redox proxies at San Giovanni show fluctuating trends within the *Chondrodonta* bedset (Fig. 5), suggesting that rapid changes in the local redox conditions and in nutrient levels did not exclude it. This finding indicates that *Chondrodonta* was resilient to variations in the seawater oxygenation. This hypothesis is confirmed by literature, where most Cretaceous monospecific (or oligo-) *Chondrodonta* biostromes are documented in low-energy, protected areas of the inner platform (Malchus *et al.*, 1995; Leonide *et al.*, 2012; Millán *et al.*, 2014; Phelps *et al.*, 2014; Núñez-Useche *et al.*, 2020, among others). Although recent studies question anoxia as a driving mechanism for the demise of rudist–coral ecosystems in the prelude of OAE1a (see Hueter *et al.*, 2020), fluctuating seawater redox conditions enabling *Chondrodonta* to outpace less tolerant benthic communities, at least at a local scale, cannot be excluded.

The stratigraphic position of the *Chondrodonta* bedsets on the ACP corresponds also to an interval of increasing water temperature in pelagic settings, far below the cooling episodes recorded within OAE1a (see Jenkyns, 2018). Although the bivalve occurs also in cooler-water settings in the Aptian (e.g. Millán

et al., 2014), warmer waters could have enhanced its proliferation before the onset of the Selli Event.

In addition to warmer and more humid conditions of the early Aptian (Erba, 1994; Weisert & Erba, 2004), changes in water chemistry (for example, salinity and pH variations) may have facilitated the *Chondrodonta* proliferation by excluding other benthic competitors and potential predators. The early dissolution of the aragonitic inner shell layer in the *Chondrodonta* bedsets of Borgo Celano has been interpreted by Posenato *et al.* (2018) as possible consequence of a different aragonite saturation state related to seawater acidification during OAE1a. Because major changes in CO₂ concentrations did not apparently result in any prolonged surface ocean acidity below or during OAE1a (see Naafs *et al.*, 2016), the seawater acidification as a cause co-favouring the flourishing of *Chondrodonta* cannot be determined nor excluded.

The geochemical proxies of the San Giovanni section (Fig. 5) also show changes towards the top of the *Chondrodonta* bedset (i.e. towards the onset of OAE1a). The relative decrease in the concentration of the RSTEs is accompanied by a dramatic drop in the P/Al ratio and by a concentration peak of Al, indicative of a terrigenous input and land-derived material (Pearce *et al.*, 2009; Westermann *et al.*, 2013; Hueter *et al.*, 2019). These combined geochemical fluctuations may reflect the exacerbation of the environmental stress on the ACP at the onset of the anoxic event, which resulted in conditions that excluded *Chondrodonta*.

Combining the stratigraphic position of the worldwide lower Aptian *Chondrodonta* accumulations below the onset of OAE1a (Fig. 12) with the increasing environmental deterioration prior to the anoxic event, it is conceivable that the proliferation of this bivalve took place in a short and confined environmental ‘window’. This window was triggered by the changing climate leading to OAE1a, which resulted in nutrient pulses promoting biotic turnover from oligotrophic to mesotrophic benthic communities in shallow-water carbonate platforms. The worldwide *Chondrodonta* accumulations occupied an environmental niche between rudist-dominated and *Bacinella*–*Lithocodium*–orbitolinid-dominated assemblages, right below the onset of OAE1a. The opportunistic behaviour of *Chondrodonta* was rather efficient in this transitional context between more stable,

stenotopic benthic communities, because the bivalve benefitted from this interval of fluctuating and increasing trophic sources.

Although increased nutrient input mainly promoted the proliferation of *Chondrodonta*, the occurrence and duration of its environmental window were also controlled by local palaeogeographic and hydrodynamic settings. Indeed, as demonstrated for the *Chondrodonta* bedsets of the ACP, low-energy, restricted and dysoxic seawater conditions allowed *Chondrodonta* to gradually flourish in monospecific biostromes close to the onset of OAE1a, outplaying the less tolerant rudists. Other environmental fluctuations (for example, seawater temperature and acidification) may also have contributed, at least locally, in outpacing the less resilient benthos.

The exacerbation of the environmental fluctuations and the extreme deterioration of the shallow-water carbonate system during the anoxic event reached the threshold for *Chondrodonta*, causing its disappearance and its final replacement by fully mesotrophic taxa like *Bacinella–Lithocodium* and orbitolinids.

CONCLUSIONS

Chondrodonta is a Cretaceous oyster-like bivalve occurring in Tethyan shallow-water carbonates, commonly found in lower Aptian strata that record considerable climate and environmental changes peaking during Oceanic Anoxic Event 1a (OAE1a). The lower Aptian *Chondrodonta* bedsets of the Apulia Carbonate Platform (ACP) can be correlated to the uppermost chemostratigraphic C2 segment of C-isotope curve straddling OAE1a. *Chondrodonta* appears within rudist limestones and reaches a brief phase of maximum proliferation in monospecific biostromes (*Chondrodonta* bedsets) that terminate abruptly right before the negative $\delta^{13}\text{C}$ excursion (C3 segment) of OAE1a. *Chondrodonta* accumulations precede the environmental stress related to the anoxic event and occupy an environmental niche between the oligo-mesotrophic (rudist-dominated) and fully mesotrophic (*Bacinella–Lithocodium*–orbitolinid-dominated) communities, as also reported worldwide.

The interval of proliferation of *Chondrodonta* on the ACP is characterized by variable nutrient levels and seawater oxygenation, and correlates also to an oligo-mesotrophic regime in the nearby pelagic realm.

Increasing nutrient loading precluding the onset of OAE1a created an environmental ‘window’ favourable for *Chondrodonta* in protected areas of the inner platform. Low energy, dysoxic seawaters and restricted circulation controlled the worldwide occurrence and duration of the environmental window. Other local to regional environmental fluctuations (for example, seawater temperature and acidification) likely contributed to the dominance of *Chondrodonta*. Further increase of inhospitable conditions leading to OAE1a inhibited the proliferation of *Chondrodonta*, allowing *Bacinella–Lithocodium* and orbitolinids to dominate within the benthic communities. The opportunistic behaviour of *Chondrodonta* was, therefore, rather efficient in the transitional context between more stable, stenotopic biotic assemblages, that occurred below the onset of OAE1a.

The proliferation of *Chondrodonta* in lower Aptian shallow-water carbonates resulted from unstable environmental conditions at the onset of OAE1a and the same is likely to apply to other Cretaceous oceanic anoxic events.

ACKNOWLEDGEMENTS

We are thankful to Dr Ulrike Weiss and Dr Brigitte Stoll (Max Plank Institute for Chemistry, Mainz, Germany) for their kind support, guidance and assistance in the LA-ICP-MS analysis. Anna Cipriani (Università di Modena e Reggio Emilia) and Silvia Riechelmann (Ruhr University Bochum) are kindly acknowledged for taking care of Sr isotopes analyses. We acknowledge Mr Renzo Tamoni for thin sections and slabs preparation. We also acknowledge the Editors Giovanna Della Porta and Gregor Eberli, and the two anonymous reviewers for their comments and suggestions which significantly improved the manuscript.

This work is a contribution to the project “*Biota resilience to global change: biomineralization of planktic and benthic calcifiers in the past, present and future*” supported by MURST (PRIN 2017RX9XXXY- GDV, MM, GF, RP), and is supported by the College of Petroleum Engineering & Geosciences, King Fahd University of Petroleum & Minerals (KR), and by the Subaward Agreement # 61725381-125201 between Stanford University and University of Ferrara (JP and MM) “*Predictive rules for the development of carbonate platforms that incorporate the combined influences of physics, chemistry, and*

biology in the formation, deposition, and early diagenesis of carbonate strata". The research was also partially supported by funding provided by Ferrara University (FAR 2017, 2018 and 2019). The authors declare that they have no competing interests that might have influenced the work described in this manuscript.

DATA AVAILABILITY STATEMENT

Data used for this study are available upon request to the corresponding author (mrh@unife.it).

REFERENCES

- Abdullah, S., Chmyriov, V.M. and Dronov, V.I. (2008) *Geology and Mineral Resources of Afghanistan*, pp. 1–488. British Geological Survey Occasional Publication No. 15, Keyworth, Nottingham, UK.
- Algeo, T.J. and Maynard, J.B. (2004) Trace-element behavior and redox facies in core shales of Upper Pennsylvanian Kansas-type cyclothems. *Chem. Geol.*, **206**, 289–318.
- Allan, J.R. and Matthews, R.K. (1982) Isotope signatures associated with early meteoric diagenesis. *Sedimentology*, **29**, 797–817. <http://doi.org/10.1111/j.1365-3091.1982.tb00085.x>
- Amodio, S. and Weissert, H. (2017) Palaeoenvironment and palaeoecology before and at the onset of Oceanic Anoxic Event (OAE)1a: reconstructions from Central Tethyan archives. *Palaeogeogr. Palaeoclimatol. Palaeoecol.*, **479**, 71–89.
- Barbieri, F., Cabdulqaadir, M.M., Di Geronimo, I., Faaduma, C.C., Giulini, P., Maxamuud, M.C.C., Michelini, G. and Piccoli, G. (1979) Il Cretaceo della regione di Hiraan in Somalia (valle dello Webi Shabelle) con appendice sulla foresta fossile di Sheekh Guure. *Sci. Geol. Mem.*, **32**, 155–182.
- Bernoulli, D. (2001) Mesozoic-Tertiary carbonate platforms, slopes and basins of the external Apennines and Sicily. In: *Anatomy of an Orogen: the Apennines and Adjacent Mediterranean Basins* (Eds Vai, G.B. and Martini, I.P.), pp. 307–326. Kluwer Academic Publishers, Lancaster.
- Bertotti, G., Casolari, E. and Picotti, V. (1999) The Gargano Promontory: a Neogene contractional belt within the Adriatic plate. *Terra Nova*, **11**, 168–173. <http://doi.org/10.1046/j.1365-3121.1999.00243.x>.
- Bodin, S., Godet, A., Matera, V., Steinmann, P., Vermeulen, J., Gardin, S., Adatte, T., Coccioni, R. and Föllmi, K.B. (2007) Enrichment of redox-sensitive trace metals (U, V, Mo, As) associated with the late Hauterivian Faraoni oceanic anoxic event. *Geol. Rundsch.*, **96**, 327–341.
- Boix, C., Frijia, G., Vicedo, V., Bernaus, J.M., Di Lucia, M., Parente, M. and Caus, E. (2011) Larger foraminifera distribution and strontium isotope stratigraphy of the La Cova limestones (Coniacian–Santonian, “Serra del Montsec”, Pyrenees, NE Spain). *Cretaceous Res.*, **32**, 806–822. <http://doi.org/10.1007/s10347-019-0565-4>.
- Bonin, A., Pucéat, E., Vennin, E., Mattioli, E., Aurell, M., Joachimski, M., Barbarin, N. and Laffont, R. (2016) Cool episode and platform demise in the Early Aptian: new insights on the links between climate and carbonate production. *Paleoceanography*, **31**, 66–80.
- Borgomano, J.R.F. (2000) The Upper Cretaceous carbonates of the Gargano-Murge region, southern Italy: a model of platform-to-basin transition. *AAPG Bull.*, **84**, 1561–1588.
- Bosellini, A., Morsilli, M. and Neri, C. (1999a) Long-term event stratigraphy of the Apulia Platform margin (Upper Jurassic to Eocene, Gargano, southern Italy). *J. Sed. Res.*, **69**, 1241–1252.
- Bosellini, A., Russo, A. and Schröder, R. (1999b) Stratigraphic evidence for an Early Aptian sea-level fluctuation: the Graua Limestone of south-eastern Ethiopia. *Cretac. Res.*, **20**, 783–791.
- Bottini, C., Erba, E., Tiraboschi, D., Jenkyns, H.C., Schouten, S. and Sinninghe Damsté, J.S. (2015) Climate variability and ocean fertility during the Aptian Stage. *Clim. Past*, **11**, 383–402. <https://doi.org/10.5194/cp-11-383-2015>.
- Bover-Arnal, T., Löser, H., Moreno-Bedmar, J.A., Salas, R. and Strasser, A. (2012) Corals on the slope (Aptian, Maestrat Basin, Spain). *Cretaceous Res.*, **37**, 43–64. <http://doi.org/10.1016/j.cretres.2012.03.001>.
- Bover-Arnal, T., Moreno-Bedmar, J.A., Salas, R., Skelton, P.W., Bitzer, K. and Gili, E. (2010) Sedimentary evolution of an Aptian syn-rift carbonate system (Maestrat Basin, E Spain): effects of accommodation and environmental change. *Geol. Acta*, **8**, 249–280.
- Bover-Arnal, T., Salas, R., Moreno-Bedmar, J.A. and Bitzer, K. (2009) Sequence stratigraphy and architecture of a late Early-Middle Aptian carbonate platform succession from the western Maestrat Basin (Iberian Chain, Spain). *Sed. Geol.*, **219**, 280–301.
- Brand, U. and Veizer, J. (1980) Chemical diagenesis of a multicomponent carbonate system-1: trace elements. *J. Sed. Petrol.*, **50**, 1219–1236. <http://doi.org/10.1306/212f7bb7-2b24-11d7-8648000102c1865d>.
- Brankman, C. and Aydin, A. (2004) Uplift and contractional deformation along a segmented strike-slip fault system: the Gargano Promontory, southern Italy. *J. Struct. Geol.*, **26**, 807–824.
- Burla, S., Heimhofer, U., Hochuli, P.A., Weissert, H. and Skelton, P. (2008) Changes in sedimentary patterns of coastal and deep-sea successions from the North Atlantic (Portugal) linked to Early Cretaceous environmental change. *Palaeogeogr. Palaeoclimatol. Palaeoecol.*, **257**, 38–57.
- Campbell, C.V. (1967) Lamina, laminaset, bed and bedset. *Sedimentology*, **8**, 7–26. <https://doi.org/10.1111/j.1365-3091.1967.tb01301.x>.
- Carras, N., Conrad, M.A. and Radoičić, R. (2006) Salpingoporella, a common genus of Mesozoic Dasycladales (calcareous green algae). *Rev. Paléobiol.*, **25**, 457–517.
- Chiocchini, M., Pampaloni, M.L. and Pichezzi, R.M. (2012) Microfacies and microfossils of the Mesozoic carbonate successions of Latium and Abruzzi (Central Italy) — Cretaceous. *Car. Geol. Ital. Mem.*, **17**, ISPPA.
- Christ, N., Immenhauser, A., Amour, F., Mutti, M., Preston, R., Whitaker, F.F., Peterhänsel, A., Egenhoff, S.O., Dunn, P.A. and Agar, S.M. (2012) Triassic Latemar cycle tops - subaerial exposure of platform carbonates under tropical arid climate. *Sed. Geol.*, **265–266**, 1–29.
- Claps, M., Parente, M., Neri, C. and Bosellini, A. (1996) Facies and cycles of the S. Giovanni Rotondo Limestone (Lower Cretaceous, Gargano Promontory, Southern Italy): the Borgo Celano section. *Ann. Univ. Ferrara*, **7**, 5–35.

- Colombie, C., Lécuyer, C. and Strasser, A. (2011) Carbon- and oxygen isotope records of palaeoenvironmental and carbonate production changes in shallow-marine carbonates (Kimmeridgian, Swiss Jura). *Geol. Mag.*, **148**, 133–153.
- Császár, G., Mhel, D., Oberhauser, R. and Lobitzer, H. (1994) A comparative study of the Urgonian Facies in Vorarlberg (Austria), in Allgäu (Germany) and in the Villány Mountains (Hungary). In: *Jubiläumsschrift 20 Jahre Geologische Zusammenarbeit Österreich-Ungarn* (Eds Lobitzer, H., Császár, G. and Daurer, A.), **2**, Wien: Geologische Bundesanstalt, 145–207.
- Damas Mollá, L., Aranburu Artano, A. and García Garmilla, F. (2006) Resistencia a la alteración diagenética de conchas de Chondrodonta sp en las calizas rojas del Aptiense-Albiense inferior de Ereño (Bizkaia). *Geogaceta*, **40**, 195–198.
- Dhondt, A.V. and Dieni, I. (1993) Non-rudistid bivalves from Late Cretaceous rudist limestones of NE Italy (Col dei Schiosi and Lago di S. Croce areas). *Sci. Geol. Mem.*, **45**, 165–241.
- Di Lucia, M., Trecalli, A., Mutti, M. and Parente, M. (2012) Bio-chemostratigraphy of the Barremian-Aptian shallow-water carbonates of the southern Apennines (Italy): pinpointing the OAE1a in a Tethyan carbonate platform. *Solid Earth*, **3**, 1–28.
- Di Palma, V. (1995) Aspetti stratigrafico-sedimentologici dei calcari di piattaforma Cretacico inferiori - Giurassico superiori del Gargano meridionale. Unpublished Degree Dissertation, University of Ferrara, Italy, 80 pp.
- Dumitrescu, M., Brassell, S.C., Schouten, S., Hopmans, E.C. and Sinninghe Damsté, J.S. (2006) Instability in tropical Pacific sea-surface temperatures during the early Aptian. *Geology*, **34**, 833–866. <http://doi.org/10.1130/g22882.1>.
- Dunham, R.J. (1962) Classification of carbonate rocks according to their depositional texture. In: *Classification of Carbonate Rocks* (Ed. Ham, W.E.s), *AAPG Mem.*, **1**, 108–121.
- Eberli, G.P., Bernoulli, D., Sanders, D. and Vecsei, A. (1993) From aggradation to progradation; the Maiella Platform, Abruzzi, Italy. In: *Cretaceous Carbonate Platforms* (Eds Simo, J.A.T., Scott, R.W. and Masse, J.-P.), *AAPG Mem.*, **56**, 213–232.
- Embry, K.O. and Klovan, J.E. (1971) A late Devonian reef tract on northeastern Banks Island, Northwestern Territories. *Bull. Can. Pet. Geol.*, **19**, 730–781.
- Erba, E. (1994) Nannofossils and superplumes: the Early Aptian “nannoconid crisis”. *Paleoceanography*, **9**, 483–501.
- Erba, E., Bottini, C., Weissert, H.J. and Keller, C.E. (2010) Calcareous Nannoplankton response to surface-water acidification around Oceanic Anoxic Event 1a. *Science*, **329**, 428–432. <http://doi.org/10.1126/science.1188886>.
- Erba, E., Channell, J.E.T., Claps, M., Jones, C., Larson, R., Opdyke, B., Premoli Silva, I., Riva, A., Salvini, G. and Torricelli, S. (1999) Integrated stratigraphy of the Cison Apticore (southern Alps, Italy); a “reference section” for the Barremian-Aptian interval at low latitudes. *J. Foram. Res.*, **29**, 371–391.
- Erba, E., Duncan, R.A., Bottini, C., Tiraboschi, D., Weissert, H., Jenkyns, H.C. and Malinverno, A. (2015) Environmental consequences of Ontong Java Plateau and Kerguelen Plateau volcanism. *Geol. Soc. Am. Spec. Pap.*, **271**–303.
- Erba, E. and Tremolada, F. (2004) Nannofossil carbonate fluxes during the early Cretaceous: phytoplankton response to nutrification episodes, atmospheric CO₂ and anoxia. *Paleoceanography*, **19**, 1–18. <http://doi.org/10.1029/2003pa000884>.
- Föllmi, K.B. (1995) 160 m. y. record of marine sedimentary phosphorus burial: coupling of climate and continental weathering under greenhouse and icehouse conditions. *Geology*, **23**, 859–862. [https://doi.org/10.1130/0091-7613\(1995\)023<0503:MYROMS>2.3.CO;2](https://doi.org/10.1130/0091-7613(1995)023<0503:MYROMS>2.3.CO;2).
- Föllmi, K.B. (1996) The phosphorus cycle, phosphogenesis and marine phosphate-rich deposits. *Earth-Sci. Rev.*, **40**, 55–124. [https://doi.org/10.1016/0012-8252\(95\)00049-6](https://doi.org/10.1016/0012-8252(95)00049-6).
- Föllmi, K.B. (2012) Early Cretaceous life, climate and anoxia. *Cretac. Res.*, **35**, 230–257.
- Föllmi, K.B., Godet, A., Bodin, S. and Linder, P. (2006) Interactions between environmental change and shallow-water carbonate buildup along the northern Tethyan margin and their impact on the Early Cretaceous carbon isotope record. *Paleoceanography*, **21**, 1–16. <http://doi.org/10.1029/2006pa001313>.
- Freneix, S. and Lefèvre, R. (1967) Deux espèces nouvelles de Chondrodonta et Neithea (Bivalves) du Sénonien du Taurus lycien (Turquie). *Bull. Soc. Géol. Fr.*, **7**, 762–776.
- Frija, G., Parente, M., Di Lucia, M. and Mutti, M. (2015) Carbon and strontium isotope stratigraphy of the Upper Cretaceous (Cenomanian-Campanian) shallow-water carbonates of southern Italy: Chronostratigraphic calibration of larger foraminifera biostratigraphy. *Cretac. Res.*, **53**, 110–139.
- Gili, E., Masse, J.-P. and Skelton, P.W. (1995) Rudists as gregarious sediment-dwellers, not reef-builders, on Cretaceous carbonate platforms. *Palaeogeogr. Palaeoclimatol. Palaeoecol.*, **118**, 245–267.
- Gili, E., Skelton, P.W., Bover-Arnal, T., Salas, R., Obrador, A. and Fenerci-Masse, M. (2016) Depositional biofacies model for post-OAE1a Aptian carbonate platforms of the western Maestrat Basin (Iberian Chain, Spain). *Palaeogeogr. Palaeoclimatol. Palaeoecol.*, **453**, 101–114.
- Giraud, F., Pittet, B., Grosheny, D., Baudin, F., Lécuyer, C. and Sakamoto, T. (2018) The palaeoceanographic crisis of the early Aptian (OAE 1a) in the Vocontian Basin (SE France). *Palaeogeogr. Palaeoclimatol. Palaeoecol.*, **511**, 483–505.
- Godet, A. (2013) Drowning unconformities: palaeoenvironmental significance and involvement of global processes. *Sed. Geol.*, **293**, 45–66.
- Godet, A., Hfaiedh, R., Arnaud-Vanneau, A., Zghal, I., Arnaud, H. and Ouali, J. (2014) Aptian palaeoclimate and identification of an OAE1a equivalent in shallow marine environments of the southern Tethyan margin: evidence from southern Tunisia (Bir Oum Ali section, Northern Chott Chain). *Cretac. Res.*, **48**, 110–129.
- Graziano, R. (2013) Sedimentology, biostratigraphy and event stratigraphy of the Early Aptian Oceanic Anoxic Event (OAE1a) in the Apulia Carbonate Platform Margin – Ionian Basin System (Gargano Promontory, southern Italy). *Cretac. Res.*, **39**, 78–111.
- Graziano, R., Raspini, A. and Spalluto, L. (2013) High resolution $\delta^{13}\text{C}$ stratigraphy through the Selli Oceanic Anoxic Event (OAE1a) in the Apulia carbonate platform: the Borgo Celano section (western Gargano Promontory, Southern Italy). *Ital. J. Geosci.*, **132**, 477–496.
- Graziano, R. and Raspini, A. (2018) High-resolution chronostratigraphy of palaeoecologic and isotopic changes in shallow-marine carbonates: deciphering the completeness of the Aptian record in the Apennine

- carbonate platform (southern Italy). *Cretac. Res.*, **86**, 97–128.
- Grotzinger, J.P., Fike, D.A. and Fischer, W.W.** (2011) Enigmatic origin of the largest-known carbon isotope excursion in Earth's history. *Nat. Geosci.*, **4**, 285–291.
- Guerzoni, S.** (2016) Analisi delle facies di piattaforma interna del Promontorio del Gargano nell'intervallo Barremiano superiore - Aptiano inferiore e confronto con le piattaforme tetidee durante l'Evento Anossico OAE1a. Ph.D. Thesis, University of Ferrara, Italy, 294 pp.
- Huck, S., Heimhofer, U., Rameil, N., Bodin, S. and Immenhauser, A.** (2011) Strontium and carbon-isotope chronostratigraphy of Barremian-Aptian shoal-water carbonates: northern Tethyan platform drowning predates OAE1a. *Earth Planet. Sci. Lett.*, **304**, 547–558. <http://doi.org/10.1016/j.epsl.2011.02.031>.
- Huck, S., Heimhofer, U., Immenhauser, A. and Weissert, H.** (2013) Carbon-isotope stratigraphy of Early Cretaceous (Urgonian) shoal-water deposits: diachronous changes in carbonate-platform production in the north-western Tethys. *Sed. Geol.*, **290**, 157–174.
- Huck, S. and Heimhofer, U.** (2015) Improving shallow-water carbonate chemostratigraphy by means of rudist bivalve sclerochemistry. *Geochem. Geophys. Geosyst.*, **16**, 3111–3128.
- Huck, S., Rameil, N., Korbar, T., Heimhofer, U., Wieczorek, T.D. and Immenhauser, A.** (2010) Latitudinally different responses of Tethyan shoal-water carbonate systems to the Early Aptian oceanic anoxic event (OAE 1a). *Sedimentology*, **57**, 1585–1614. <http://doi.org/10.1111/j.1365-3091.2010.01157.x>.
- Huck, S., Stein, M., Immenhauser, A., Skelton, P.W., Christ, N., Föllmi, K.B. and Heimhofer, U.** (2014) Response of proto-North Atlantic carbonate-platform ecosystems to OAE1a-related stressors. *Sed. Geol.*, **313**, 15–31.
- Huck, S., Wohlwend, S., Coimbra, R., Christ, N. and Weissert, H.** (2017) Disentangling shallow-water bulk carbonate carbon isotope archives with evidence for multi-stage diagenesis: an in-depth component-specific petrographic and geochemical study from Oman (mid-Cretaceous). *Depositional Record*, **3**, 233–257. <http://doi.org/10.1002/dep2.35>.
- Hueter, A., Huck, S., Bodin, S., Heimhofer, U., Weyer, S., Jochum, K.P. and Immenhauser, A.** (2019) Central Tethyan platform-top hypoxia during Oceanic Anoxic Event 1a. *Climate Past Discuss.*, **15**, 1327–1344. <http://doi.org/10.5194/cp-15-1327-2019>.
- Hueter, A., Huck, S., Heimhofer, U., Bodin, S., Weyer, S., Jochum, K.P., Roebbert, Y. and Immenhauser, A.** (2020) Evaluating the role of coastal hypoxia on the transient expansion of microencruster intervals during the early Aptian. *Lethaia*, <https://doi.org/10.1111/let.12411>.
- Husinec, A., Harman, C.A., Regan, S.P., Mosher, D.A., Sweeney, R.J. and Read, J.F.** (2012) Sequence development influenced by intermittent cooling events in the Cretaceous Aptian greenhouse, Adriatic platform, Croatia. *Am. Assoc. Pet. Geol. Bull.*, **96**, 2215–2244.
- Husinec, A. and Read, J.F.** (2011) Microbial laminite versus rooted and burrowed caps on peritidal cycles: salinity control on parasequence development, Early Cretaceous isolated carbonate platform, Croatia. *Geol. Soc. Am. Bull.*, **123**, 1896–1907.
- Husinec, A. and Read, J.F.** (2018) Cyclostratigraphic and $\delta^{13}\text{C}$ record of the Lower Cretaceous Adriatic Platform, Croatia: assessment of Milankovitch-forcing. *Sed. Geol.*, **373**, 11–31.
- Immenhauser, A., Della Porta, G., Kenter, J.A.M. and Bahamonde, J.R.** (2003) An alternative model for positive shifts in shallow-marine carbonate $\delta^{13}\text{C}$ and $\delta^{18}\text{O}$. *Sedimentology*, **50**, 953–959. <http://doi.org/10.1046/j.1365-3091.2003.00590.x>.
- Immenhauser, A., Hillgärtner, H., Sattler, U., Bertotti, B., Schoepfer, P., Homewood, P., Vahrenkamp, V., Steuber, T., Masse, J.-P., Droste, H.H.J., van Koppen, J., van der Kooij, B., van Bentum, E.C., Verwer, K., Hoogerduijn-Strating, E., Swinkels, W., Peters, P., Immenhauser-Potthast, I. and Al Maskery, S.A.J.** (2004) Barremian-lower Aptian Qishn Formation, Haushi-Huqf area, Oman: a new outcrop analogue for the Kharaiib/Shu'aiba reservoirs. *GeoArabia*, **9**, 153–194.
- Immenhauser, A., Hillgärtner, H. and van Bentum, E.** (2005) Microbial-foraminiferal episodes in the Early Aptian of the southern Tethyan margin: ecological significance and possible relation to oceanic anoxic event 1a. *Sedimentology*, **52**, 77–99. <http://doi.org/10.1111/j.1365-3091.2004.00683.x>.
- Immenhauser, A., Holmden, C. and Patterson, W.P.** (2008) Interpreting the carbon-isotope record of ancient shallow epeiric seas: Lessons from the recent. In: *Dynamics of Epeiric Seas* (Eds Holmden, C. and Pratt, B.W.). *Geol. Assoc. Can. Spec. Publ.*, **48**, 137–174.
- Insalaco, E.** (1998) The descriptive nomenclature and classification of growth fabrics in fossil scleractinian reefs. *Sed. Geol.*, **118**, 159–186.
- Jenkyns, H.C.** (2003) Evidence for rapid climate change in the Mesozoic-Palaeogene greenhouse world. *Phil. Trans. Roy. Soc. London A*, **361**, 1885–1916. <http://doi.org/10.1098/rsta.2003.1240>.
- Jenkyns, H.C.** (2010) Geochemistry of oceanic anoxic events. *Geochem. Geophys. Geosyst.*, **11**, 1–30.
- Jenkyns, H.C.** (2018) Transient cooling episodes during Cretaceous Oceanic Anoxic Events with special reference to OAE1a (Early Aptian). *Phil. Trans. Roy. Soc. London*, **376**, 1–26. <http://doi.org/10.1098/rsta.2017.0073>.
- Larson, R.L.** (1991) Geological consequences of superplumes. *Geology*, **19**, 933–966. [https://doi.org/10.1130/0091-7613\(1991\)019<0963:GCOS>2.3.CO;2](https://doi.org/10.1130/0091-7613(1991)019<0963:GCOS>2.3.CO;2).
- Larson, R.L. and Erba, E.** (1999) Onset of the mid-Cretaceous greenhouse in the Barremian-Aptian: igneous events and the biological, sedimentary and geochemical responses. *Paleoceanography*, **14**, 663–678. <http://doi.org/10.1029/1999pa900040>.
- Leonide, P., Borgomano, J., Masse, J.-P. and Doublet, S.** (2012) Relation between stratigraphic architecture and multi-scale heterogeneities in carbonate platforms: the Barremian-lower Aptian of the Monts de Vaucluse, SE France. *Sed. Geol.*, **265**, 87–109.
- Lohmann, K.C.** (1988) Geochemical patterns of meteoric diagenetic systems and their application to studies of paleokarst. In: *Paleokarst* (Eds James, N.P. and Choquette, P.W.), pp. 58–80. Springer Verlag, New York, NY.
- Lokier, S.W. and Al Junaihi, M.** (2016) The petrographic description of carbonate facies: are we all speaking the same language? *Sedimentology*, **63**, 1843–1885. <http://doi.org/10.1111/sed.12293>.
- Luciani, V., Cobianchi, M. and Jenkyns, H.C.** (2001) Biotic and geochemical response to anoxic events: the Aptian pelagic succession of the Gargano Promontory (southern Italy). *Geol. Mag.*, **138**, 277–298.
- Luciani, V., Cobianchi, M. and Lupi, C.** (2006) Regional record of a global oceanic anoxic event: OAE1a on the

- Apulia Platform margin, Gargano Promontory, southern Italy. *Cretac. Res.*, **27**, 754–772.
- Luperto Sinni, E.** and **Masse, J.-P.** (1986) Données nouvelles sur la stratigraphie del calcaires de plate-forme du Crétacé inférieur du Gargano (Italie méridionale). *Riv. Ital. Paleontol. Stratigr.*, **92**, 33–66.
- Malchus, N., Pons, J.M.** and **Salas, R.** (1995) Rudist distribution in the Lower Aptian shallow platform of La Mola de Xert, eastern Iberian Range, NE Spain. *Rev. Mex. Cienc. Geol.*, **12**, 224–235.
- Malinverno, A., Erba, E.** and **Herbert, T.D.** (2010) Orbital tuning as an inverse problem: chronology of the early Aptian oceanic anoxic event 1a (Selli Level) in the Cismon Apticore. *Paleoceanography*, **25**, 1–16. <http://doi.org/10.1029/2009pa001769>.
- Masse, J.-P.** (1993) Valanginian–early Aptian carbonate platforms from Provence, southeastern France. In: *Cretaceous Carbonate Platforms* (Eds Simo, J.A.T., Scott, R.W. and Masse, J.-P.), *AAPG Mem.*, **56**, 363–374.
- Masse, J.-P.** and **Fenerci-Masse, M.** (2013) Drowning events, development and demise of carbonate platforms and controlling factors: the Late Barremian–Early Aptian record of southeast France. *Sed. Geol.*, **298**, 28–52.
- Masse, J.-P., Fenerci-Masse, M., Özer, S., Güngör, T.** and **Akal, C.** (2015) Berriasian rudist faunas and micropalaeontology of Stramberk type carbonate exotics from the Lycian nappes, Bodrum Peninsula, southwest Turkey. *Cretac. Res.*, **56**, 76–92.
- Maurer, F., van Buchem, F.S.P., Eberli, G.P., Pierson, B.J., Raven, M.J., Larsen, P.-H., Al-Husseini, M.I.** and **Vincent, B.** (2013) Late Aptian long-lived glacio-eustatic lowstand recorded on the Arabian Plate. *Terra Nova*, **25**, 87–94. <http://doi.org/10.1111/ter.12009>.
- McArthur, J.M., Howarth, R.J.** and **Bailey, T.R.** (2001) Strontium Isotope Stratigraphy: Lowess version 3: best fit to the marine Sr-isotope curve for 0–509 Ma and accompanying look-up table for deriving numerical age. *J. Geol.*, **109**, 155–170. <http://doi.org/10.1086/319243>.
- McArthur, J.M., Howarth, R.J.** and **Shields, G.A.** (2012) Strontium isotope stratigraphy. In: *The Geologic Time Scale 2012* (Eds Gradstein, F.M., Ogg, J.G., Schmitz, M. and Ogg, G.), pp. 127–144. Elsevier, Amsterdam.
- McArthur, J.M., Mutterlose, J., Price, G.D., Rawson, P.F., Ruffell, A.** and **Thirwall, M.F.** (2004) Belemnites of Valanginian, Hauterivian and Barremian age: Sr-isotope stratigraphy, composition ($^{87}\text{Sr}/^{86}\text{Sr}$, $\delta^{13}\text{C}$, $\delta^{18}\text{O}$, Na, Sr, Mg) and palaeo-oceanography. *Palaeogeogr. Palaeoclimatol. Palaeoecol.*, **202**, 253–272.
- Méhay, S., Keller, C.E., Bernasconi, S.M., Weissert, H., Erba, E., Bottini, C.** and **Hochuli, P.A.** (2009) A volcanic CO₂ pulse triggered the Cretaceous Oceanic Anoxic Event 1a and a biocalcification crisis. *Geology*, **37**, 819–822. <http://doi.org/10.1130/g30100a.1>.
- Menegatti, A.P., Weissert, H., Brown, R.S., Tyson, R.V., Farrimond, P., Strasser, A.** and **Caron, M.** (1998) High-resolution $\delta^{13}\text{C}$ stratigraphy through the Early Aptian “Livello Selli” of the Alpine Tethys. *Paleoceanography*, **13**, 530–545. <http://doi.org/10.1029/98pa01793>.
- Millán, M.I., Weissert, H.J., Fernández-Mendiola, P.A.** and **García-Mondéjar, J.** (2009) Impact of Early Aptian carbon cycle perturbations on evolution of a marine shelf system in the Basque-Cantabrian Basin (Aralar, N Spain). *Earth Planet. Sci. Lett.*, **287**, 392–401. <http://doi.org/10.1016/j.epsl.2009.08.023>.
- Millán, M.I., Weissert, H.J., Owen, H., Fernández-Mendiola, P.A.** and **García-Mondéjar, J.** (2011) The Madotz Urgonian platform (Aralar, northern Spain): paleoecological changes in response to Early Aptian global environmental events. *Palaeogeogr. Palaeoclimatol. Palaeoecol.*, **312**, 167–180.
- Millán, M.I., Weissert, H.J.** and **López-Horgue, M.A.** (2014) Expression of the late Aptian cold snaps and the OAE1b in a highly subsiding carbonate platform (Aralar, northern Spain). *Palaeogeogr. Palaeoclimatol. Palaeoecol.*, **411**, 167–179.
- Morsilli, M.** and **Bosellini, A.** (1997) Carbonate facies zonation of the Upper Jurassic–Lower Cretaceous Apulia platform margin (Gargano Promontory, Southern Italy). *Riv. Ital. Paleontol. Stratigr.*, **103**, 193–206.
- Morsilli, M., Hairabian, A., Borgomano, J., Nardon, S., Adams, E.** and **Gartner, G.B.** (2017) The Apulia Carbonate Platform—Gargano Promontory, Italy (Upper Jurassic–Eocene). *AAPG. Bull.*, **101**, 523–531. <http://doi.org/10.1306/011817dig17031>.
- Mutti, M.** and **Hallock, P.** (2003) Carbonate systems along nutrient and temperature gradients: some sedimentological and geochemical constraints. *Int. J. Earth Sci.*, **92**, 465–475. <http://doi.org/10.1007/s00531-003-0350-y>.
- Naafs, B.D.A., Castro, J.M., De Gea, G.A., Quijano, M.L., Schmidt, D.N.** and **Pancost, R.D.** (2016) Gradual and sustained carbon dioxide release during Aptian Oceanic Anoxic Event 1a. *Nat. Geosc.*, **9**, 135–139.
- Najarro, M., Rosales, I.** and **Martín-Chivelet, J.** (2010) Major palaeoenvironmental perturbation in an Early Aptian carbonate platform: prelude of the oceanic anoxic event 1a? *Sed. Geol.*, **235**, 50–71.
- Najarro, M., Rosales, I.** and **Martín-Chivelet, J.** (2011) Major palaeoenvironmental perturbation in an Early Aptian carbonate platform: prelude of the Oceanic Anoxic Event 1a? *Sed. Geol.*, **235**, 50–71.
- Núñez-Useche, F., Barragán, R., Torres-Martínez, M.A., López-Zúñiga, P.A., Moreno-Bedmar, J.A., Chávez-Cabello, G., Canet, C.** and **Chacon-Baca, E.** (2020) Response of the western proto-North Atlantic margin to the early Aptian oceanic anoxic event (OAE) 1a: an example from the Cupido platform margin–Gulf of Mexico, NE Mexico. *Cretac. Res.*, **113**, 104488. <http://doi.org/10.1016/j.cretres.2020.104488>.
- Oehlert, A.M.** and **Swart, P.K.** (2014) Interpreting carbonate and organic carbon isotope covariance in the sedimentary record. *Nat. Commun.*, **5**, 1–7.
- Oehlert, A.M.** and **Swart, P.K.** (2019) Rolling window regression of $\delta^{13}\text{C}$ and $\delta^{18}\text{O}$ values in carbonate sediments: Implications for source and diagenesis. *Depositional Record*, **5**, 613–630. <http://doi.org/10.1002/dep2.88>.
- Ogg, J.G.** and **Hinnov, L.A.** (2012) Cretaceous. In: *The Geologic Time Scale 2012* (Eds Gradstein, F.M., Ogg, J.G., Schmitz, M. and Ogg, G.M.), pp. 793–853. Elsevier, Amsterdam.
- Pancost, R.D., Crawford, N., Magness, S., Turner, A., Jenkyns, H.C.** and **Maxwell, J.R.** (2004) Further evidence for the development of photic-zone euxinic conditions during Mesozoic Oceanic Anoxic Events. *J. Geol. Soc. London*, **161**, 353–364. <http://doi.org/10.1144/0016764903-059>.
- Parente, M., Frijia, G.** and **Di Lucia, M.** (2007) Carbon-isotope stratigraphy of Cenomanian–Turonian platform carbonates from the southern Apennines (Italy): a chemostratigraphic approach to the problem of correlation between shallow-water and deep-water successions. *J.*

- Geol. Soc. London.*, **164**, 609–620. <http://doi.org/10.1144/0016-76492006-010>.
- Patterson, W.P. and Walter, L.M.** (1994) Depletion in ^{13}C in seawater ΣCO_2 on modern carbonate platforms: significance for the carbon isotopic record of carbonate. *Geology*, **22**, 885–888. [https://doi.org/10.1130/0091-7613\(1994\)022<0885:DOCISC>2.3.CO;2](https://doi.org/10.1130/0091-7613(1994)022<0885:DOCISC>2.3.CO;2).
- Pearce, M.A., Jarvis, I. and Tocher, B.A.** (2009) The Cenomanian – Turonian boundary event, OAE2 and palaeoenvironmental change in epicontinental seas: New insights from the dinocyst and geochemical records. *Palaeogeogr. Palaeoclimatol. Palaeoecol.*, **280**, 207–234.
- Petti, F.M., Conti, M.A., D’Orazi Porchetti, S., Morsilli, M., Nicosia, U. and Gianolla, P.** (2008) A theropod dominated ichnocoenosis from late Hauterivian-early Barremian of Borgo Celano (Gargano Promontory, Apulia, southern Italy). *Riv. Ital. Paleontol. Stratigr.*, **114**, 3–17.
- Phelps, R.M., Kerans, C., Loucks, R.G., Da-Gama, R.O.B.P., Jeremiah, J. and Hull, D.** (2014) Oceanographic and eustatic control of carbonate platform evolution and sequence stratigraphy on the Cretaceous (Valanginian – Campanian) passive margin, northern Gulf of Mexico. *Sedimentology*, **61**, 461–496. <http://doi.org/10.1111/sed.12062>.
- Phelps, R.M., Kerans, C., Da-Gama, R.O.B.P., Jeremiah, J., Hull, D. and Loucks, R.G.** (2015) Response and recovery of the Comanche carbonate platform surrounding multiple Cretaceous oceanic anoxic events, northern Gulf of Mexico. *Cretac. Res.*, **54**, 117–144. <http://doi.org/10.1016/j.cretres.2014.09.002>.
- Pictet, A., Delanoy, G., Adatte, T., Spangenberg, J.E., Baudouin, C., Boselli, P., Boselli, M., Kindler, P. and Föllmi, K.B.** (2015) Three successive phases of platform demise during the early Aptian and their association with the oceanic anoxic Selli episode (Ardèche, France). *Palaeogeogr. Palaeoclimatol. Palaeoecol.*, **418**, 101–125.
- Pittet, B., van Buchem, F.S.P., Hillgärtner, H., Razin, P., Grötsch, J. and Droste, H.** (2002) Ecological succession, palaeoenvironmental change, and depositional sequences of Barremian-Aptian shallow-water carbonates in northern Oman. *Sedimentology*, **49**, 555–581. <http://doi.org/10.1046/j.1365-3091.2002.00460.x>.
- Posenato, R., Frijia, G., Morsilli, M., Moro, A., Del Viscio, G. and Mezga, A.** (2020) Palaeoecology and proliferation of the bivalve *Chondrodonta joannae* (Choffat) in the upper Cenomanian (Upper Cretaceous) Adriatic Carbonate Platform of Istria (Croatia). *Palaeogeogr. Palaeoclimatol. Palaeoecol.*, **548**, 109703.
- Posenato, R., Morsilli, M., Guerzoni, S. and Bassi, D.** (2018) Palaeoecology of *Chondrodonta* (Bivalvia) from the lower Aptian (Cretaceous) Apulia Carbonate Platform (Gargano Promontory, southern Italy). *Palaeogeogr. Palaeoclimatol. Palaeoecol.*, **508**, 188–201.
- Pratt, B.R. and Smewing, J.D.** (1990) Jurassic and Early Cretaceous platform margin configuration and evolution, central Oman Mountains. *Geol. Soc. London. Spec. Publ.*, **49**, 69–88. <http://doi.org/10.1144/gsl.sp.1992.049.01.06>.
- Prokoph, A., Shields, G.A. and Veizer, J.** (2008) Compilation and time-series analysis of a marine carbonate $\delta^{18}\text{O}$, $\delta^{13}\text{C}$, $^{87}\text{Sr}/^{86}\text{Sr}$ and $\delta^{34}\text{S}$ database through Earth history. *Earth-Science Rev.*, **87**, 113–133. <http://doi.org/10.1016/j.earscirev.2007.12.003>.
- Rameil, N., Immenhauser, A., Warrlich, G., Hillgärtner, H. and Droste, H.J.** (2010) Morphological patterns of Aptian Lithocodium-Bacinella geobodies: relation to environment and scale. *Sedimentology*, **57**, 883–911. <http://doi.org/10.1111/j.1365-3091.2009.01124.x>.
- Schlanger, S.O. and Jenkyns, H.C.** (1976) Cretaceous oceanic anoxic events: causes and consequences. *Geol. en Mijnb.*, **55**, 179–184.
- Schmitt, K., Heimhofer, U., Frijia, G., Di Lucia, M. and Huck, S.** (2020) Deciphering the fragmentary nature of Cretaceous shallow-water limestone archives: a case study from the subtropical Apennine carbonate platform. *Newsletters Stratigr.*, **53**, 389–413. <http://doi.org/10.1127/nos/2019/0551>.
- Schröder, R., van Buchem, F.S.P., Cherchi, A., Baghbani, D., Vincent, B., Immenhauser, A. and Granier, B.** (2010) Revised orbitolinid biostratigraphic zonation for the Barremian-Aptian of the eastern Arabian Plate and implications for regional stratigraphic correlations. *GeoArabia Spec. Publ.*, **4**, 49–96.
- Scott, R.W. and Finch, R.C.** (1999) Cretaceous carbonate biostratigraphy and environments in Honduras. In: *Sedimentary Basins of the World, Caribbean Sedimentary Basins* (Eds Mann, P. and Hsu, K.J.), pp. 151–165. Elsevier, Amsterdam.
- Shields, G. and Stille, P.** (2001) Diagenetic constraints on the use of cerium anomalies as palaeoseawater redox proxies: an isotopic and REE study of Cambrian phosphorites. *Chem. Geol.*, **175**, 29–48. [http://doi.org/10.1016/s0009-2541\(00\)00362-4](http://doi.org/10.1016/s0009-2541(00)00362-4).
- Sholkovitz, E.R. and Schneider, D.L.** (1991) Cerium redox cycles and rare earth elements in the Sargasso Sea. *Geochim. Cosmochim. Acta*, **55**, 2737–2743. [http://doi.org/10.1016/0016-7037\(91\)90440-g](http://doi.org/10.1016/0016-7037(91)90440-g).
- Skelton, P.W. and Gili, E.** (2012) Rudists and carbonate platforms in the Aptian: a case study on biotic interactions with ocean chemistry and climate. *Sedimentology*, **59**, 81–117. <http://doi.org/10.1111/j.1365-3091.2011.01292.x>.
- Stanton, T.W.** (1901) *Chondrodonta*, a new genus of ostreiform mollusks from the Cretaceous, with descriptions of the genotype and a new species. *Nat. Mus. Proc.*, **24**, 301–307.
- Stein, M., Westermann, S., Adatte, T., Matera, V., Fleitmann, D., Spangenberg, J.E. and Föllmi, K.B.** (2012) Late Barremian-Early Aptian palaeoenvironmental change: the Cassis-La Bédoule section, southeast France. *Cretaceous Res.*, **37**, 209–222. <http://doi.org/10.1016/j.cretres.2012.03.021>.
- Steuber, T., Korbar, T., Jelaska, V. and Gusić, I.** (2005) Strontium-isotope stratigraphy of Upper Cretaceous platform carbonates of the island of Brač (Adriatic Sea, Croatia): implications for global correlation of platform evolution and biostratigraphy. *Cretaceous Res.*, **26**, 741–756. <http://doi.org/10.1016/j.cretres.2005.04.004>.
- Swart, P.K. and Oehlert, A.M.** (2018) Revised interpretations of stable C and O patterns in carbonate rocks resulting from meteoric diagenesis. *Sed. Geol.*, **364**, 14–23.
- Tejada, M.L.G., Suzuki, K., Kuroda, J., Coccioni, R., Mahoney, J.J., Ohkouchi, N., Sakamoto, T. and Tatsumi, Y.** (2009) Ontong Java Plateau eruption as a trigger for the early Aptian oceanic anoxic event. *Geology*, **37**, 855–858. <http://doi.org/10.1130/g25763a.1>.
- Theiling, B.P., Railsback, L.B., Holland, S.M. and Crowe, D.E.** (2007) Heterogeneity in geochemical expression of subaerial exposure in limestones, and its implications for sampling to detect exposure surfaces. *J. Sed. Res.*, **77**, 159–169. <http://doi.org/10.2110/jsr.2007.014>.
- Tribouillard, N., Algeo, T.J., Lyons, T. and Riboulleau, A.** (2006) Trace metals as paleoredox and paleoproductivity proxies: An update. *Chem. Geol.*, **232**, 12–32.

- Ullmann, C.V. and Korte, C. (2015) Diagenetic alteration in low-Mg calcite from macrofossils: a review. *Geol. Quarterly*, **59**, 3–20. <http://doi.org/10.7306/gq.1217>.
- Vahrenkamp, V.C. (2010) Chemostratigraphy of the Lower Cretaceous Shu'aiba Formation: a $\delta^{13}\text{C}$ reference profile for the Aptian Stage from the southern Neo-Tethys Ocean. In: *Barremian – Aptian stratigraphy and hydrocarbon habitat of the eastern Arabian Plate*. (Eds van Buchem, F.S.P., Al-Husseini, M.I., Maurer, F. and Droste, H.J.), *GeoArabia Spec. Publ.*, **4**, 107–138.
- Velić, I. (2007) Stratigraphy and Palaeobiogeography of Mesozoic Benthic Foraminifera of the Karst Dinarides (SE Europe). *Geol. Croat.*, **60**, 1–113.
- Vilas, L., Masse, J.P. and Arias, C. (1995) Orbitolina episodes in carbonate platform evolution: the early Aptian model from SE Spain. *Palaeogeogr. Palaeoclimatol. Palaeoecol.*, **119**, 35–45.
- Weissert, H. and Erba, E. (2004) Volcanism, CO_2 and palaeoclimate: a Late Jurassic–Early Cretaceous carbon and oxygen isotope record. *J. Geol. Soc. London*, **161**, 695–702. <http://doi.org/10.1144/0016-764903-087>.
- Weissert, H., Lini, A., Föllmi, K.B. and Kuhn, O. (1998) Correlation of Early Cretaceous isotope stratigraphy and platform drowning events: a possible link? *Palaeogeogr. Palaeoclimatol. Palaeoecol.*, **137**, 189–203.
- Westermann, S., Stein, M., Matera, V., Fiet, N., Fleitmann, D., Adatte, T. and Föllmi, K.B. (2013) Rapid changes in the redox conditions of the western Tethys Ocean during the early Aptian oceanic anoxic event. *Geochim. Cosmochim. Acta*, **121**, 467–486. <http://doi.org/10.1016/j.gca.2013.07.023>.
- Wissler, L., Funk, H. and Weissert, H. (2003) Response of Early Cretaceous carbonate platforms to changes in atmospheric carbon dioxide levels. *Palaeogeogr. Palaeoclimatol. Palaeoecol.*, **200**, 187–205.
- Zaghib-Turki, D. (2003) Cretaceous coral-rudist formations in Tunisia. In: *North African Cretaceous Carbonate Platform Systems* (Eds Gili, E., Negra, M.E.H. and Skelton, P.W.), pp. 83–110. Springer Netherlands, Dordrecht.

Manuscript received 23 September 2020; revision accepted 6 April 2021

Supporting Information

Additional information may be found in the online version of this article:

Supporting Information. Procedures and analytical methods for the geochemical analyses performed in this study. The entire geochemical dataset, of both stable isotopes and trace elements, is also included.